A&A 406, 579–592 (2003)
DOI: 10.1051/0004-6361:20030825
© ESO 2003

Astronomy & Astrophysics

Multi-frequency study of the B3-VLA sample

III. Polarisation properties

U. Klein[1], K.-H. Mack[2,3,1], L. Gregorini[2,4], and M. Vigotti[2]

[1] Radioastronomisches Institut der Universität Bonn, Auf dem Hügel 71, 53121 Bonn, Germany
[2] Istituto di Radioastronomia del CNR, Via Gobetti 101, 40129 Bologna, Italy
[3] ASTRON, Postbus 2, 7990 AA Dwingeloo, The Netherlands
[4] Dipartimento di Fisica, Università di Bologna, Via Irnerio 46, 40126 Bologna, Italy

Received 10 April 2003 / Accepted 19 May 2003

Abstract. This paper is the third of a series, and presents the results of the linear polarisation of the B3-VLA sample, at 1.4, 2.7, 4.8 and 10.5 GHz. We find that flat-spectrum sources are significantly less polarised than the steep ones at 10.5 GHz. A trend is seen for sources with larger linear size to be more strongly polarised. Compact steep-spectrum sources (CSSs) exhibit much stronger depolarisation than non-CSSs. Flat-spectrum sources are characterized by almost constant, and low, degrees of polarisation over the whole wavelength range studied here. We add 143 new Rotation Measures to the available database published by Wielebinski & Krause (1993). An important result is that the decrease of the degree of polarisation is almost linear with wavelength and does not drop to zero at lower frequencies. This behaviour cannot be fitted by any existing model of external depolarisation or intrinsic Faraday dispersion.
We consider an intrinsic process producing the observed depolarisation, involving three source components with different emissivities and Faraday depths, while the Faraday rotation must arise from a foreground screen, most likely Galactic in origin.

Key words. polarisation – surveys – radio continuum: galaxies

1. Introduction

The B3-VLA survey (Vigotti et al. 1989) has produced a large multi-frequency database as a subsample of radio sources from the B3 survey (Ficarra et al. 1985). The B3-VLA sample consists of 1049 radio sources in five flux-limited subsamples stronger than 0.1 Jy at 408 MHz. Subsequent measurements with the Effelsberg 100-m telescope at cm wavelengths (Gregorini et al. 1998, Paper I; Vigotti et al. 1999, Paper II) extended the frequency range to 151 MHz through 10.5 GHz, allowing detailed spectral studies of a sample exceeding 1000 sources. This paper is the third of a series, and presents the properties of the linear polarisation of the detected sources. Linear polarisation was detected for a fair subsample of the B3-VLA survey at 1.4, 2.695, 4.85 and 10.5 GHz, where measurements at 2.695 GHz have been recently conducted in order to properly sample the frequency base.

Studies of radio source polarisation have a number of important aspects. First, they serve to disclose polarisation properties intrinsic to the sources, either statistically or via high-resolution observations of individual sources. Synchrotron emission in combination with Faraday effects which modify the polarisation properties is the most powerful tool for such investigations, in particular if measured with a good sampling over a sufficiently large frequency range. Measurements of large samples of radio sources can also be utilized to study the magneto-ionic properties of the foreground medium, viz. the magnetized interstellar medium (ISM) of the Milky Way. The latter route to the study of the Galactic magnetic field has been taken by a number of authors and was pioneered by the work of Kronberg & Simard-Normandin (1976) and by Sofue et al. (1979). The last update of the available database of Rotation Measures (*RM*s) of 976 extragalactic radio sources has been published by Wielebinski & Krause (1993). Whenever a survey of radio sources with polarisation measurements at a sufficient number of frequencies is carried out, the polarisation results should be added as a "byproduct" to the existing database. With this paper, we add 143 RMs, which according to the right ascension and declination constraints of the B3-VLA survey are distributed over two strips stretching in the range $115^\circ < l_{\rm II} < 146^\circ$, $-24^\circ < b_{\rm II} < -12^\circ$, and $23^\circ < l_{\rm II} < 73^\circ$, $150^\circ < b_{\rm II} < 185^\circ$.

In Sect. 2 we describe the observations and data reduction only in brief, since the details have been presented in the preceding papers. In Sect. 3 we present the database of linear polarisation, along with a description of the derivation

Send offprint requests to: U. Klein,
e-mail: uklein@astro.uni-bonn.de

Article published by EDP Sciences and available at http://www.aanda.org or http://dx.doi.org/10.1051/0004-6361:20030825

of the polarisation parameters and their errors from the observed Stokes parameters, at each frequency. In Sect. 4 the results are presented, comparing with other work of this kind. The polarisation properties are analyzed and discussed in the light of Faraday effects extrinsic or intrinsic to the Milky Way. Section 5 summarizes the results.

2. The observations

The observations reported here have been carried out between July 1994 and October 2000. The observations at 10.5 and 4.85 GHz were described in detail in Papers I and II.

For the sources with detected polarisation at 10.5 GHz we used the Effelsberg 100-m telescope to get full polarisation information at 2.7 GHz. These observations were carried out in April and in October 2000. The 2.7-GHz system has one feed in the secondary focus of the 100-m telescope followed by a two channel total-power system, with HEMT amplifiers in the first stage. The system is connected to an IF-polarimeter providing full linear polarisation information with Stokes parameters I, Q, and U. The system operates at a centre frequency of 2.695 GHz, the bandwidth is 40 MHz. The system temperature was $\sim$40 K on the sky (zenith).

Due to the half-power beam width of $261''$ all sources were observed by cross-scanning the telescope in right ascension and declination, with a scan length of $24'$. In the case of slightly extended sources the cross scans were oriented with one scan direction along the source major axes (e.g. along double or triple components). This orientation was taken from the VLA maps of Vigotti et al. (1989). The scanning speed was $60'$/min, in total between 16 and 24 subscans were made for each source in order to get close to the confusion limit for polarisation at 2.7 GHz. Standard calibration sources were cross-scanned in regular intervals with two cross-scans each to check the telescope pointing and flux density scale. For the latter purpose the primary calibrators were 3C 286 and 3C 295, with 3C 48 and 3C 138 being used as secondaries. The exact flux density scale for each target source was applied by checking two subsequent observations of calibration sources. The calibrated flux densities are on the flux density scale of Baars et al. (1977). The fractional polarisation and the polarisation angle were checked by comparing the measured values of strongly polarised calibrators (3C 286, 3C 48, 3C 138) with the catalogues of Simard-Normandin et al. (1981). Typical errors were found to be $\pm 0.5\%$ for fractional polarisation and $\pm 1^\circ$ for the polarisation angle. The unpolarised planetary nebula NGC 7027 was observed to check the amount of instrumental polarisation which was found to be 1%.

3. Polarisation database

The observed sample is defined by the 192 sources with significant polarisation at 10.5 GHz (for brevity hereafter referred to as *the polarised sample*), the highest radio frequency at which the entire B3-VLA survey has completely been observed. Since depolarisation tends to have stronger effects at lower frequencies, the largest number of polarised sources is expected to be found at 10.5 GHz. A source was defined to show a significant detection if Stokes I and either Stokes Q or U yielded a measured value above 3-$\sigma_{\rm rms}$. The database also contains measurements of linear polarisation at 2.7 and 4.8 GHz (Effelsberg), and were combined with corresponding data derived from the maps of the NRAO VLA Sky Survey (NVSS, Condon et al. 1998).

3.1. Data obtained from the NVSS (1.4 GHz)

Small cutouts from the NVSS IQU-cubes centred on the B3-VLA positions have been obtained for the entire sample. Using AIPS task *BLSUM* the integrated flux densities of all Stokes parameters were determined. This warrants the determination of these parameters over equal regions. When determining flux densities from maps by pixel integration the errors consist of three components:

- a calibration error ($\Delta S_{\rm c}$): the calibration error of the NVSS has been estimated $\lesssim$3% (Condon et al. 1998);
- a noise error ($\Delta S_{\rm n}$): this component depends on the size of the integration area $A_{\rm int}$ (the integration area in units of the beam solid angle) and the rms noise σ of the map as $\Delta S_{\rm n} = \sigma\sqrt{A_{\rm int}}$;
- a possibly wrong zero level ($\Delta S_{\rm z}$): this component depends also on the size of the area (in units of solid angle $A_{\rm z}$ in which the zero level is determined: $\Delta S_{\rm z} = \sigma\frac{A_{\rm int}}{\sqrt{A_{\rm z}}}$. This error can usually be neglected for interferometer maps.

Hence, the total measurement error is calculated as

$$\Delta S_i = \sqrt{(S_i \cdot \Delta S_{\rm c})^2 + \Delta S_{\rm n}^2 + \Delta S_{\rm z}^2} \qquad \text{for} \quad i = I, Q, U,$$

where S_i is the flux density in mJy.

3.2. Data obtained with the Effelsberg telescope (2.7 GHz, 4.8 GHz, 10.5 GHz)

The analysis of our cross-scan observations has been described in detail by Gregorini et al. (1998). The values for Stokes Q and U are obtained as for Stokes I. The errors are produced by the uncertainties of the calibration $\Delta S_{\rm c}$, by the local noise $\Delta S_{\rm n}$ and due to source confusion $\Delta S_{\rm conf}$. The total error for cross-scans is calculated as

$$\Delta S_i = \sqrt{(S_i \cdot \Delta S_{\rm c})^2 + \Delta S_{\rm n}^2 + \Delta S_{\rm conf}^2} \qquad \text{for} \quad i = I, Q, U.$$

In Table 1 we have compiled the values used to compute the errors of polarisation parameters and the values of the instrumental polarisation for the different frequencies. Here, σ denotes the rms noise in the cross-scans, calculated in the emission-free portions. The confusion in Stokes U and Q at $\lambda\lambda$11 and 6.3 cm has been estimated from the behaviour of the rms noise in cross scans with very long integrations.

3.3. Determination of the polarisation parameters

Based on the Stokes parameters and their errors the polarisation parameters have been calculated for each of the measured

Table 1. Values used to compute the errors of polarisation parameters and values of the instrumental polarisation.

Frequency		I		U/Q		$P_{\rm instr}$
	$\Delta S_{\rm c}$	σ	$\Delta S_{\rm conf}$	σ	$\Delta S_{\rm conf}$	
[GHz]		[mJy]	[mJy]	[mJy]	[mJy]	[%]
1.4	0.03	0.45	–	0.29	–	0.3
2.7	0.02	2.1	1.5	1.1	0.5	1.0
4.8	0.02	1.0	0.45	0.3	0.15	0.7
10.5	0.02	0.8	0.08	0.4	–	1.5

frequencies. The polarised flux density, $S_{\rm p}$, and its error are:

$$S_{\rm p} = \sqrt{S_Q^2 + S_U^2} \qquad \Delta S_{\rm p} = \frac{\sqrt{(S_Q \cdot \Delta S_Q)^2 + (S_U \cdot \Delta S_U)^2}}{S_{\rm p}}.$$

At 1.4 GHz where this parameter is determined from maps a correction to the positive noise bias has been applied. In this case, $S_{\rm p}$ has been calculated according to

$$S_{\rm p} = \sqrt{S_Q^2 + S_U^2 - (1.2 \cdot \sigma_{QU})^2} \text{ where } \sigma_{QU} = \sqrt{\sigma_Q^2 + \sigma_U^2}.$$

The factor 1.2 has been found empirically (Wardle & Kronberg 1974; Mack et al. 1997). The Effelsberg cross-scans do not require a correction since S_Q and S_U are determined by fits to the data which take the influence of noise into account.

The fractional polarisation m is calculated via

$$m = S_{\rm p}/S_I \qquad \Delta m = \sqrt{(\Delta S_{\rm p}/S_I)^2 + (S_{\rm p} \cdot \sigma_I/S_I^2)^2}.$$

The polarisation angle χ is obtained as

$$\chi = 0.5 \cdot \arctan \frac{S_U}{S_Q} \qquad \Delta\chi = 0.5 \cdot \frac{\sigma_{QU}}{S_{\rm p}}.$$

In Table 3 we present the measured polarisation data of the B3-VLA sample containing 192 sources with detected polarisation at 10.5 GHz. An asterisk indicates sources belonging to the complete sample (see Sect. 4.1). For each source we list the polarised flux density, the polarisation percentage and the polarisation angle with their errors, respectively, at 1.4, 2.7, 4.8 and 10.5 GHz. For completeness we have also included the new flux densities at 2.7-GHz with their errors.

4. Discussion of polarisation properties

4.1. Percentage of polarisation and depolarisation

The sample containing the 192 radio sources with detected polarisation at 10.5 GHz is not complete: sources with $S < 80$ mJy at 10.5 GHz are present only if the polarisation percentage is high enough to be detected. Therefore, a bias is inherent to this sample towards sources with a high polarisation percentage. From this sample we extracted a *complete sample* which consists of all the sources with total flux densities large enough to allow detection of their linear polarisation at 10.5 GHz with the 100-m telescope. In this sample, which contains 208 sources with total flux densities above 80 mJy at 10.5 GHz, 106 radio sources have been detected in polarisation (indicated with an asterisk in Table 3). The median percentage of polarisation is 1.5%, comparable to the instrumental polarisation at this frequency.

Table 2. Median degrees of polarisation of the "complete sample" at all four frequencies.

All sources		
ν	Median	Error
[GHz]	[%]	[%]
1.4	1.9	0.2
2.7	3.4	0.2
4.8	4.1	0.3
10.5	4.6	0.3
Steep spectrum sources		
1.4	2.2	0.6
2.7	3.7	0.2
4.8	5.2	0.3
10.5	5.8	0.4
Flat spectrum sources		
1.4	1.6	0.4
2.7	2.4	0.4
4.8	2.6	0.4
10.5	2.5	0.4

In Fig. 1 the histograms of the polarisation percentage (m) at four frequencies are shown. The shadowed histograms represent sources with spectral index flatter than -0.5 ($S_\nu \propto \nu^\alpha$), which henceforth we refer to as the flat-spectrum sample. The median of m for *all* sources and for steep- and flat-spectrum sources is compiled in Table 2. Comparing m at the four frequencies for sources with flat and steep spectra, it is clear that the difference for the two groups of sources is strong at 10.5 GHz (the median values are 3% and 6% for sources with flat and steep spectra, respectively), becoming almost equal at lower frequencies (median values are about 2% at 1.4 GHz; see also Sect. 4.1 in Saikia & Salter 1988).

The polarisation percentage correlates with the linear size of the sources; in fact the median linear size of the sources with high m (i.e. greater than the median m of the sample) is about 7 times greater than that of sources with low m, independent of wavelength. For example at 10.5 GHz the sources with $m > 4.6\%$ have a median linear size of 14^{+3}_{-2} kpc, the sources with lower m ($<4.6\%$) have a median linear size of $1.7^{+2.5}_{-1.1}$ kpc (Strom 1973).

It is not surprising that the median size of flat spectrum sources is smaller than the median size of steep spectrum sources, because flat spectrum sources are synchrotron self-absorbed and thus quite compact. The low polarisation correlates with both the spectral index and the linear size; at present we cannot establish which is the fundamental correlation.

We have computed the depolarisation for the 106 detected sources of the complete sample, defined as

$$DP = \frac{m_{\nu_1}}{m_{\nu_2}}.$$

Between 1.4 and 10.5 GHz we have obtained a median value of 0.53, taking into account the upper limits. Dividing the sample into radio sources with $\log P_{1.4} > 27.3$ W Hz^{-1} and

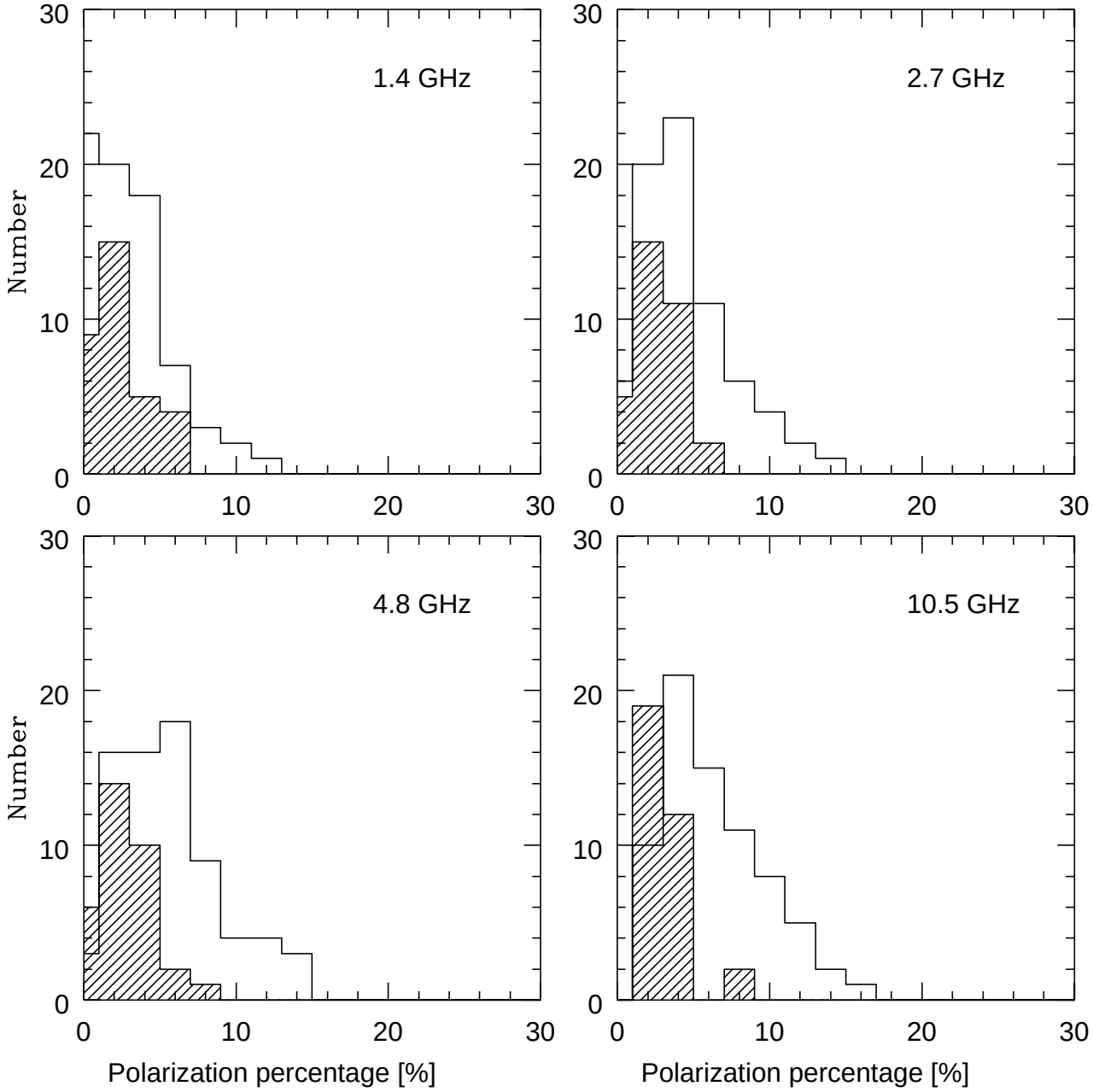

Fig. 1. Polarisation percentage at 1.4, 2.7, 4.85 and 10.5 GHz. At each frequency the shadowed histogram represents sources with spectral index flatter than -0.5, the other histogram is for those with steeper spectra.

$\log P_{1.4} < 27.3$ W Hz^{-1} we have found no difference in the depolarisation. This was already found out by Mesa et al. (2002), who utilized our database to work out predictions for any possible contamination of future measurements of the linear polarisation of the cosmic microwave background.

Collecting information on the properties of Compact Steep-Spectrum Sources (CSSs) is of particular interest. This population has been described in terms of two models: the youth scenario, i.e. they could reflect an early stage in the evolution of radio sources (Fanti et al. 1995), or the frustration scenario, i.e. they are inhibited from growing to larger sizes by unusual conditions in the interstellar medium of their host galaxies (van Breugel et al. 1984). We have considered the sample of 92 sources with $S_{408\,\mathrm{MHz}} > 0.8$ Jy extracted from the 106 detected sources with the same limiting flux adopted for the B3-VLA CSS sample (Fanti et al. 2001). The depolarisation of the CSSs is much stronger than that of the non-CSSs. The 79 non-CSSs show a depolarisation of $0.57^{+0.1}_{-0.1}$, while the 13 CSSs have a depolarisation ranging from 0 to 0.6 with a median value of $0^{+0.1}_{-0}$.

4.2. The Rotation Measure

The polarisation angle (χ) measured at different wavelengths permits us to derive the Rotation Measure in rad m^{-2},

$$RM = 0.81 \int_0^{s_0} \frac{n_\mathrm{e}}{\mathrm{cm}^{-3}} \cdot \frac{B_{||}}{\mu\mathrm{G}} \cdot \frac{\mathrm{d}s}{\mathrm{pc}}$$

Table 3. Polarisation data at 1.4 GHz, 2.7 GHz, 4.85 GHz and 10.5 GHz.

Name		1.4 GHz						2.7 GHz								4.8 GHz						10.5 GHz					
		S_p	ΔS_p		m	Δm	χ	$\Delta\chi$	S	ΔS	S_p	ΔS_p		m	Δm	χ	$\Delta\chi$	S_p	ΔS_p		m	Δm	χ	$\Delta\chi$	S_p	ΔS_p	m	Δm	χ	$\Delta\chi$
		[mJy]			[%]		[°]		[mJy]		[mJy]			[%]		[°]		[mJy]			[%]		[°]		[mJy]		[%]		[°]	
0010+405	*	34.5	1.6		2.1	0.1	81.5	0.5	1165.4	25.7	24.2	0.9		2.1	0.1	5.6	1.8	6.9	0.2		0.8	0.0	48.3	3.0	13.1	1.6	1.6	0.2	64.5	6.9
0013+387		10.2	1.1		3.8	0.4	164.3	1.6	145.5	4.3	9.4	0.6		6.5	0.5	54.9	5.2	3.6	0.4		4.4	0.4	97.9	5.9	4.0	1.3	9.6	3.0	125.0	16.4
0022+390	*	33.2	1.6		4.6	0.2	12.4	0.5	660.2	15.1	26.0	1.1		3.9	0.2	20.7	2.0	20.0	0.4		3.4	0.1	75.5	3.0	20.2	1.2	4.1	0.3	87.1	3.3
0022+394		0.0	0.0	<	2.5	0.0	0.0	0.0	29.3	2.2	2.9	0.7		9.9	2.6	145.6	14.8	0.0	0.0	<	5.4	0.0	0.0	3.0	1.9	0.6	14.8	5.0	33.2	15.5
0029+394		6.0	1.3		1.5	0.3	98.7	2.8	212.7	5.7	5.7	0.7		2.7	0.3	112.7	6.5	8.7	0.2		7.6	0.2	159.2	3.0	3.6	1.2	8.3	2.7	174.4	16.3
0032+423		0.0	0.0	<	1.2	0.0	0.0	0.0	194.0	5.0	4.2	0.9		2.2	0.5	103.7	10.9	3.6	0.2		3.3	0.2	59.4	3.0	5.5	1.5	9.2	2.5	29.2	13.7
0041+382A		11.5	1.5		5.1	0.7	155.2	1.4	108.0	4.1	7.4	1.4		6.9	1.3	189.0	9.7	6.5	0.4		11.6	0.6	49.3	3.9	3.4	1.0	19.1	5.5	81.0	17.7
0041+393		11.5	1.3		7.7	0.9	176.6	1.4	87.6	2.1	10.8	0.9		12.3	1.1	179.2	5.0	5.9	0.4		10.6	0.6	48.8	3.8	4.0	0.7	15.8	3.0	79.3	11.1
0042+386		10.5	1.5		4.4	0.6	25.0	1.6	88.1	2.4	0.0	0.0	<	3.9	0.0	0.0	0.0	1.7	0.3		3.8	0.6	47.4	8.7	2.1	0.7	12.4	3.9	80.9	20.7
0045+404		21.9	1.5		9.5	0.7	12.9	0.8	129.2	3.3	17.0	0.7		13.2	0.6	170.6	2.7	10.2	0.3		13.4	0.5	31.3	3.2	6.2	1.4	21.9	5.2	39.2	10.4
0051+404	*	19.6	1.9		2.2	0.2	96.4	0.8	467.1	10.7	15.2	1.1		3.3	0.3	113.3	4.0	15.1	0.3		6.2	0.2	178.5	3.0	8.3	1.2	7.5	1.1	21.6	8.5
0052+395		6.4	1.3		4.4	0.9	54.8	2.6	104.2	4.4	3.2	0.9		3.1	0.9	175.2	17.9	1.5	0.8		3.6	1.1	53.0	17.9	1.9	0.6	7.9	2.7	58.9	17.9
0057+395		10.8	1.1		14.3	1.5	67.9	1.5	43.8	2.0	16.0	1.3		36.4	3.4	69.0	5.2	6.5	0.3		23.9	1.2	114.9	3.5	4.3	1.4	28.7	9.2	140.2	13.5
0059+461	*	51.5	2.0		4.0	0.2	38.4	0.3	651.9	16.0	35.5	1.3		5.4	0.2	156.8	1.9	16.5	0.3		5.7	0.2	12.3	3.0	4.7	1.7	4.2	1.7	39.5	19.7
0105+441		8.7	1.5		2.1	0.4	67.2	1.9	224.4	5.8	10.4	1.2		4.6	0.6	191.9	6.1	6.9	0.2		5.0	0.2	57.3	3.0	3.5	0.9	4.5	1.1	71.9	13.6
0109+416B		5.9	1.8		0.7	0.2	56.3	2.8	463.9	10.2	18.7	1.3		4.0	0.3	153.2	4.3	7.9	0.4		3.2	0.1	51.2	3.4	4.9	1.2	8.2	2.0	87.1	15.0
0110+401	*	21.0	1.6		3.8	0.3	110.8	0.8	361.0	9.9	8.1	1.9		2.2	0.5	52.7	17.7	9.8	0.2		4.2	0.1	82.1	3.0	8.8	1.2	6.1	0.9	99.0	8.0
0113+400	*	9.8	1.3		1.4	0.2	179.2	1.7	386.9	10.2	25.5	1.2		6.6	0.4	44.0	2.9	16.9	0.3		8.5	0.2	96.1	3.0	9.8	1.4	10.5	1.6	114.0	8.6
0115+453A	*	5.1	1.4		0.4	0.1	122.4	3.3	639.3	13.3	8.6	1.0		1.4	0.2	30.5	6.0	11.1	1.1		3.2	0.2	65.2	5.2	6.6	1.5	4.6	1.0	80.7	11.2
0116+438		7.6	1.5		1.7	0.3	8.7	2.2	255.4	5.7	21.3	2.1		8.3	0.8	97.7	3.9	18.3	0.5		12.2	0.4	123.7	3.1	8.9	1.9	12.6	3.1	131.6	10.7
0128+394		0.0	0.0	<	0.0	0.0	0.0	0.0	163.0	5.6	0.0	0.0	<	4.9	0.0	0.0	0.0	1.7	0.4		2.0	0.4	95.9	8.5	5.1	1.2	20.5	5.1	123.9	13.0
0130+381	*	8.3	1.2		1.9	0.3	15.7	2.0	283.1	8.2	8.6	1.3		3.0	0.5	25.0	8.7	4.8	0.2		2.8	0.1	43.8	3.0	4.3	1.6	4.1	1.6	35.9	17.5
0133+381		0.0	0.0	<	2.0	0.0	0.0	0.0	85.0	2.1	5.1	1.0		6.0	1.2	57.3	10.7	4.2	0.3		9.3	0.7	82.5	4.5	2.3	0.7	10.7	3.5	82.7	11.5
0139+389A		5.0	1.1		2.3	0.5	126.3	3.4	129.5	5.3	5.6	1.2		4.3	1.0	94.8	11.8	3.1	0.2		3.7	0.2	144.5	3.0	2.9	1.1	6.9	2.6	169.5	19.4
0149+398		11.7	1.4		4.1	0.5	57.6	1.4	193.5	4.9	13.3	1.0		6.9	0.5	15.3	3.9	5.6	0.2		4.8	0.2	60.9	3.0	3.6	0.7	4.5	1.0	85.9	11.3
0152+435	*	85.8	3.0		4.6	0.2	48.3	0.2	994.0	21.4	31.5	1.1		3.2	0.1	25.6	1.6	10.9	0.5		2.2	0.1	40.9	3.3	8.6	0.8	3.4	0.3	59.5	5.5
0153+417	*	39.4	2.0		5.1	0.3	53.2	0.4	407.2	10.0	14.1	2.4		3.5	0.6	185.5	10.6	11.6	0.3		5.7	0.2	52.2	3.0	7.7	1.8	7.7	1.8	60.8	12.3
0157+442	*	16.5	1.6		1.3	0.1	142.2	1.0	695.2	17.1	41.0	1.1		5.9	0.2	173.2	1.5	23.7	0.4		6.8	0.2	60.8	3.0	6.9	1.5	4.7	1.1	71.0	11.0
0201+396		0.0	0.0	<	1.6	0.0	0.0	0.0	24.4	3.2	6.0	1.0		24.6	5.3	184.1	8.6	0.0	0.0	<	12.2	0.0	0.0	3.0	0.9	0.2	20.9	7.1	37.9	15.6
0202+380		16.7	1.6		8.9	0.8	96.0	1.0	104.5	2.9	7.0	1.4		6.7	1.4	44.2	9.8	6.7	0.4		9.7	0.7	95.3	4.5	5.0	0.8	11.9	2.0	113.0	10.1
0213+392		10.0	1.3		9.1	1.2	101.9	1.7	56.6	2.5	5.4	1.5		9.5	2.7	138.8	13.8	3.3	0.3		10.9	0.9	172.0	4.2	1.3	0.3	9.2	2.4	159.5	15.7
0213+412	*	0.0	0.0	<	0.3	0.0	0.0	0.0	335.2	9.4	6.4	1.0		1.9	0.3	179.7	9.0	3.7	0.2		1.9	0.1	83.3	3.0	4.3	0.9	3.7	0.8	76.7	12.6
0216+423	*	34.1	1.8		4.3	0.2	164.8	0.5	438.0	9.4	23.7	1.0		5.4	0.3	139.6	2.5	12.6	0.3		5.7	0.2	176.7	3.0	5.4	0.9	4.6	0.8	31.8	9.4
0218+396	*	34.9	1.9		3.6	0.2	175.3	0.5	500.1	12.3	24.8	1.6		5.0	0.3	147.9	3.3	12.9	0.6		5.2	0.2	9.5	3.4	16.0	1.9	10.2	1.3	30.4	6.6
0219+428A	*	40.2	1.8		1.7	0.1	49.4	0.4	1882.0	38.9	10.1	1.5		0.7	0.1	70.3	17.0	24.0	1.0		1.8	0.1	159.5	3.2	18.5	2.3	1.5	0.2	179.6	7.3
0220+393A	*	12.2	1.4		2.3	0.3	28.8	1.4	353.5	8.0	7.8	1.1		2.2	0.3	46.6	8.1	3.4	0.7		1.4	0.2	78.9	8.3	3.4	1.2	2.0	0.7	85.6	19.3
0220+397	*	25.2	1.9		0.8	0.1	123.1	0.7	1602.9	35.4	142.2	3.0		8.9	0.3	111.2	0.6	105.0	1.8		14.4	0.4	149.7	3.0	40.0	1.4	13.8	0.6	163.3	1.7
0224+396		3.4	1.1		4.8	1.6	105.5	4.9	40.4	2.8	3.4	0.7		8.4	1.9	136.0	12.6	6.0	0.2		19.4	0.6	165.1	3.0	1.6	0.3	13.9	3.0	186.8	13.3
0243+439		23.2	1.5		4.9	0.3	161.3	0.7	282.8	6.7	20.0	0.9		7.1	0.4	80.4	2.3	12.2	0.3		7.7	0.2	108.4	3.0	7.1	1.4	8.9	1.9	129.2	10.5
0246+392		5.2	1.3		2.5	0.6	155.4	3.2	136.5	4.3	4.2	1.0		3.1	0.7	46.8	13.6	2.2	0.3		2.7	0.3	70.4	6.2	3.6	1.1	9.9	3.3	88.7	20.5

Table 3. continued.

Name		1.4 GHz						2.7 GHz								4.8 GHz						10.5 GHz					
		S_p [mJy]	ΔS_p		m [%]	Δm	χ [°]	$\Delta\chi$	S [mJy]	ΔS	S_p [mJy]	ΔS_p		m [%]	Δm	χ [°]	$\Delta\chi$	S_p [mJy]	ΔS_p		m [%]	Δm	χ [°]	$\Delta\chi$	S_p [mJy]	ΔS_p	m [%]	Δm	χ [°]	$\Delta\chi$
0247+404		15.6	1.3		4.4	0.4	63.5	1.1	203.7	5.0	18.7	1.0		9.2	0.5	9.5	2.8	10.6	0.2		10.3	0.3	41.4	3.0	7.9	1.4	17.0	3.0	58.1	9.6
0250+384		15.5	1.3		3.7	0.3	28.7	1.1	194.2	5.1	13.3	1.1		6.9	0.6	106.8	4.7	6.9	0.3		7.9	0.3	136.6	3.8	2.6	0.5	8.7	1.8	128.8	11.7
0251+393	*	9.6	1.4		4.0	0.6	26.8	1.7	223.7	5.2	6.5	1.0		2.9	0.5	114.3	9.3	9.8	0.2		2.9	0.1	139.9	3.0	9.3	1.2	2.3	0.3	160.4	7.0
0258+443		13.8	1.5		3.2	0.3	50.5	1.2	247.5	5.7	15.4	1.1		6.2	0.5	169.0	3.9	10.1	0.2		7.3	0.2	10.2	3.0	7.7	1.5	11.2	2.3	26.2	10.1
0707+380A		0.0	0.0	<	0.6	0.0	0.0	0.0	101.7	3.0	0.0	0.0	<	3.4	0.0	0.0	0.0	1.6	0.0	<	3.6	0.0	0.0	3.0	1.2	0.3	6.8	1.8	127.9	13.7
0710+457	*	18.0	1.7		1.4	0.1	69.2	0.9	760.8	16.4	13.2	1.1		1.7	0.1	65.7	4.1	17.0	0.7		3.6	0.1	56.1	3.3	6.0	1.0	2.4	0.4	64.9	9.9
0723+397		9.1	1.2		5.8	0.8	106.9	1.8	80.2	2.5	7.5	1.0		9.4	1.3	84.1	6.5	4.8	0.3		10.1	0.7	65.5	4.1	1.6	0.5	7.3	2.6	41.2	16.8
0736+400		28.7	1.3		12.4	0.6	79.1	0.6	131.3	4.2	18.5	0.9		14.1	0.8	75.9	2.5	13.3	0.5		15.6	0.9	72.9	3.3	9.6	1.6	24.7	4.3	74.5	9.5
0739+397B	*	3.6	1.1		0.7	0.2	68.7	4.7	390.3	9.1	4.5	0.8		1.2	0.2	38.6	14.0	8.1	0.6		2.8	0.1	44.7	3.8	5.5	1.5	2.2	0.6	51.4	11.8
0739+398	*	5.8	1.1		4.5	0.8	70.0	2.9	115.7	3.4	4.7	1.2		4.1	1.1	37.5	15.2	3.2	0.5		2.9	0.4	57.7	7.2	4.6	0.8	4.8	0.9	59.0	9.8
0742+394		7.8	1.1		5.5	0.7	47.4	2.1	79.5	2.1	10.0	0.7		12.6	1.0	53.2	4.3	6.5	0.3		15.8	0.8	57.1	3.5	2.5	0.5	19.1	4.2	43.1	10.7
0743+392B		0.0	0.0	<	1.0	0.0	0.0	0.0	150.4	5.4	13.9	1.0		9.2	0.7	52.7	4.1	12.9	0.5		14.8	0.7	36.5	3.2	5.0	0.5	18.5	2.0	32.8	4.6
0751+392		17.2	1.2		5.9	0.4	22.8	1.0	178.0	3.9	18.8	1.0		10.6	0.6	171.9	2.3	12.7	0.5		13.2	0.5	167.2	3.4	9.3	1.2	20.2	2.7	161.7	7.7
0754+396		43.7	1.8		7.8	0.3	91.6	0.4	268.7	6.2	21.2	1.0		7.9	0.4	81.2	2.3	14.8	0.5		10.0	0.4	76.9	3.1	9.7	1.1	19.8	2.4	81.7	7.3
0756+377	*	10.9	1.6		0.6	0.1	88.1	1.5	853.8	17.9	9.3	0.8		1.1	0.1	37.3	5.9	39.4	0.9		8.4	0.2	8.1	3.0	21.2	1.0	12.3	0.6	5.0	2.7
0800+472	*	5.0	1.1		0.5	0.1	89.6	3.3	518.6	11.5	3.5	0.7		0.7	0.1	117.9	12.3	4.5	0.5		1.4	0.1	138.7	5.2	4.1	1.5	2.4	0.9	158.0	17.1
0805+406	*	26.4	1.5		4.9	0.3	36.2	0.6	319.0	6.8	18.7	1.3		5.9	0.4	170.3	2.8	14.3	0.5		7.1	0.3	160.3	3.2	8.5	1.6	7.7	1.5	144.1	9.7
0806+426	*	11.0	1.6		0.5	0.1	42.4	1.5	1141.3	24.1	28.8	1.2		2.5	0.1	35.6	1.9	39.2	0.9		6.2	0.2	61.3	3.0	10.6	1.8	5.9	1.0	127.4	9.9
0809+404	*	0.0	0.0	<	0.1	0.0	0.0	0.0	644.1	13.9	2.7	0.8		0.7	0.1	125.2	19.1	5.6	0.5		1.4	0.1	33.9	7.2	9.8	1.4	5.0	0.7	53.7	8.0
0811+388		25.2	1.6		4.6	0.3	37.3	0.7	275.9	6.8	19.1	1.0		6.9	0.4	9.9	2.8	9.8	0.5		6.6	0.3	6.8	3.4	4.3	1.3	8.2	2.8	174.7	19.2
0814+425	*	33.6	1.8		3.0	0.2	103.9	0.5	1044.7	22.5	37.0	1.1		3.5	0.1	87.9	1.2	11.2	0.6		0.7	0.0	59.0	4.5	39.8	1.5	3.7	0.2	93.8	1.9
0818+472A	*	30.9	1.4		1.7	0.1	156.4	0.5	1033.7	24.1	39.7	1.3		3.8	0.2	158.9	1.2	27.7	1.0		4.5	0.2	167.3	3.2	8.3	1.9	4.2	1.0	169.6	11.2
0820+431	*	5.9	1.5		0.6	0.2	144.5	2.8	478.7	10.6	16.8	0.9		3.5	0.2	141.6	2.9	10.5	0.6		4.2	0.2	150.3	3.5	3.1	0.7	3.0	0.7	144.7	11.8
0821+394	*	89.1	2.9		5.8	0.2	143.4	0.2	1126.6	31.4	70.6	1.7		6.3	0.2	122.4	0.8	36.4	0.6		3.2	0.1	102.4	3.0	43.5	1.7	2.5	0.1	77.0	2.1
0821+447	*	25.0	1.6		3.4	0.2	110.3	0.7	393.9	9.7	18.5	0.9		4.7	0.3	101.5	2.6	9.4	0.5		4.2	0.2	92.4	3.7	3.0	0.8	3.1	0.9	77.7	14.0
0827+378	*	21.7	1.7		0.9	0.1	9.8	0.8	1407.8	29.7	47.2	1.2		3.4	0.1	133.1	1.1	10.3	0.9		1.1	0.1	38.2	4.5	23.2	1.1	4.7	0.2	184.3	3.5
0836+426	*	9.4	1.6		1.7	0.3	172.4	1.8	378.3	8.4	8.2	1.1		2.2	0.3	147.6	7.3	11.6	0.6		3.5	0.2	170.8	3.6	6.7	1.8	3.2	0.9	147.7	13.8
0841+386	*	4.2	1.3		1.0	0.3	40.1	3.9	323.8	7.2	11.2	1.1		3.5	0.4	170.7	4.9	6.8	0.3		3.2	0.1	131.2	3.0	12.0	1.6	4.9	0.7	51.6	8.0
0841+403		46.0	1.9		11.2	0.5	31.6	0.4	224.4	5.2	24.8	1.2		11.1	0.6	5.9	2.4	14.7	0.5		11.5	0.4	177.6	3.1	5.0	1.4	9.2	3.0	186.7	16.1
0849+394		0.0	0.0	<	6.1	0.0	0.0	0.0	23.0	1.9	0.0	0.0	<	16.2	0.0	0.0	0.0	3.9	0.2		29.7	1.3	64.0	3.0	1.4	0.3	22.6	7.4	86.6	15.6
0849+424		17.2	1.2		3.7	0.3	22.0	1.0	242.5	5.6	8.1	0.8		3.4	0.4	22.3	6.0	6.4	0.2		4.6	0.2	48.8	3.0	1.7	0.5	3.0	0.9	12.8	13.5
0852+384		8.3	1.1		4.7	0.6	141.6	2.0	94.6	3.2	7.3	1.0		7.8	1.1	111.5	7.8	3.1	0.3		6.0	0.4	99.4	4.2	1.3	0.6	5.3	2.5	105.8	24.9
0854+399B		38.3	2.0		7.6	0.4	52.6	0.4	230.0	5.3	16.4	0.8		7.1	0.4	20.7	2.4	12.5	0.9		8.9	0.8	11.1	5.8	5.0	1.3	7.1	1.8	178.0	13.2
0857+391	*	17.7	1.3		3.5	0.3	120.3	0.9	307.6	6.8	11.5	1.1		3.7	0.4	92.0	6.0	11.1	0.6		5.9	0.3	74.7	3.3	4.6	0.8	5.3	1.0	68.0	9.6
0858+452	*	24.6	1.3		2.9	0.1	114.4	0.7	466.7	10.5	15.5	0.8		3.3	0.2	51.7	3.1	24.4	0.6		9.1	0.3	23.6	3.1	11.5	1.1	11.0	1.1	24.1	5.4
0859+470	*	23.7	1.4		1.3	0.1	22.4	0.7	1410.2	30.6	33.4	1.1		2.4	0.1	80.3	1.5	5.2	0.2		0.7	0.0	136.5	3.0	15.9	1.3	1.7	0.1	126.7	4.6
0900+428	*	65.7	2.2		5.2	0.2	14.0	0.3	866.2	19.6	37.7	1.0		4.4	0.1	179.7	1.2	38.5	0.8		4.1	0.1	176.0	3.1	14.4	1.7	3.2	0.4	166.5	6.2
0904+417B	*	75.2	2.7		5.0	0.2	150.8	0.2	805.0	21.4	40.6	1.4		5.0	0.2	105.5	1.7	24.6	0.7		5.4	0.2	81.5	3.1	14.6	1.2	7.3	1.0	77.2	7.4
0905+380A	*	41.0	1.8		1.9	0.1	28.8	0.4	1008.0	21.6	38.5	1.2		3.8	0.1	13.1	1.5	26.7	0.6		5.7	0.2	21.9	3.0	9.3	1.6	5.8	1.0	19.2	9.6

Table 3. continued.

Name		1.4 GHz						2.7 GHz								4.8 GHz						10.5 GHz					
		S_p	ΔS_p		m	Δm	χ	$\Delta\chi$	S	ΔS	S_p	ΔS_p		m	Δm	χ	$\Delta\chi$	S_p	ΔS_p	m	Δm	χ	$\Delta\chi$	S_p	ΔS_p	m	Δm	χ	$\Delta\chi$
		[mJy]			[%]		[°]		[mJy]		[mJy]			[%]		[°]		[mJy]		[%]		[°]		[mJy]		[%]		[°]	
0906+383		7.3	1.0		3.8	0.5	72.8	2.3	107.1	3.5	4.5	1.0		4.2	1.0	37.1	13.4	2.6	0.3	4.6	0.5	43.3	5.4	1.2	0.3	5.9	1.6	35.0	16.4
0906+430	*	9.9	1.7		0.2	0.0	67.4	1.7	2348.3	50.8	21.3	0.9		0.9	0.0	88.4	2.3	27.7	0.6	1.8	0.1	78.8	3.0	16.9	1.3	1.5	0.1	148.0	4.9
0907+381	*	0.0	0.0	<	0.5	0.0	0.0	0.0	218.7	4.9	5.2	1.1		2.4	0.5	160.7	9.5	4.7	0.4	3.5	0.2	144.3	4.0	7.7	1.5	7.2	1.4	163.6	10.4
0911+395		0.0	0.0	<	0.8	0.0	0.0	0.0	68.9	2.1	0.0	0.0	<	5.2	0.0	0.0	0.0	2.2	0.3	6.0	0.6	178.6	6.4	1.2	0.3	7.5	2.0	168.7	15.5
0911+418	*	61.4	2.3		12.7	0.5	142.4	0.3	298.9	6.5	42.7	1.3		14.3	0.5	161.5	1.3	27.5	0.7	14.3	0.4	168.8	3.0	17.9	1.2	15.7	1.1	163.3	3.8
0913+385		21.4	1.3		6.5	0.4	130.0	0.8	218.8	5.3	19.0	0.9		8.7	0.4	109.3	2.6	13.3	0.5	9.6	0.3	96.6	3.2	6.3	1.9	10.0	3.2	90.2	14.8
0913+391	*	11.1	2.0		1.1	0.2	38.1	1.5	740.9	16.4	19.1	1.0		2.6	0.1	38.2	2.8	31.3	0.6	4.4	0.1	35.7	3.1	10.7	1.6	2.2	0.3	30.8	8.0
0918+381	*	27.5	1.5		3.3	0.2	46.3	0.6	432.9	9.7	26.5	1.3		6.1	0.3	153.2	2.6	11.2	0.4	4.8	0.2	147.8	3.4	6.8	1.2	6.0	1.4	140.8	11.7
0919+381		3.9	1.3		1.3	0.4	25.4	4.3	0.0	0.0	0.0	0.0	<	0.0	0.0	0.0	0.0	2.7	0.8	3.4	0.7	130.0	11.4	6.4	1.6	22.9	5.7	0.1	15.5
0922+407	*	5.1	1.3		1.8	0.5	6.8	3.3	333.8	7.6	0.0	0.0	<	1.5	0.0	0.0	0.0	4.2	0.4	1.5	0.1	36.5	4.0	5.6	1.2	1.7	0.4	190.4	11.3
0922+422		0.0	0.0	<	1.2	0.0	0.0	0.0	124.8	4.0	3.4	0.9		2.7	0.7	124.3	18.5	5.3	0.4	8.3	0.6	146.8	4.5	4.1	1.5	19.6	7.3	125.5	17.5
0923+392	*	12.3	1.9		0.4	0.1	56.0	1.4	6389.9	138.0	0.0	0.0	<	0.9	0.0	0.0	0.0	71.4	1.1	0.7	0.0	27.5	3.0	602.0	16.9	5.0	0.2	130.3	1.1
0936+405		41.4	1.6		6.9	0.3	104.4	0.4	282.2	6.1	32.3	1.0		11.5	0.4	96.7	1.4	20.2	0.7	14.5	0.5	94.7	3.1	6.2	1.5	14.9	3.9	128.8	15.0
0937+391	*	54.7	2.0		8.0	0.3	76.9	0.3	382.8	9.6	38.1	2.0		10.0	0.6	45.5	2.3	24.2	0.6	11.3	0.3	41.4	3.1	10.5	1.5	10.1	1.8	52.1	9.7
0945+408	*	91.8	2.8		5.6	0.2	29.5	0.2	1981.0	42.8	78.0	1.6		3.9	0.1	26.3	0.9	61.1	1.6	3.2	0.1	24.9	3.1	22.3	1.2	1.6	0.1	141.6	3.4
0951+422	*	0.0	0.0	<	0.3	0.0	0.0	0.0	266.6	6.1	0.0	0.0	<	2.3	0.0	0.0	0.0	2.5	0.4	1.6	0.2	155.1	7.1	5.6	2.2	5.1	2.0	147.2	17.6
0955+380		0.0	0.0	<	1.7	0.0	0.0	0.0	61.3	2.4	0.0	0.0	<	6.3	0.0	0.0	0.0	1.0	0.3	3.7	0.8	61.2	10.0	1.5	0.4	13.5	4.1	46.9	17.6
0955+390		18.6	1.7		3.9	0.4	40.9	0.9	264.3	5.9	20.3	1.8		7.7	0.7	178.2	4.4	10.3	0.4	6.6	0.3	179.1	3.3	6.8	1.6	11.5	2.7	188.6	12.9
1004+446	*	46.1	2.3		3.3	0.2	39.0	0.4	781.8	17.4	32.6	1.0		4.2	0.2	27.5	1.6	20.6	1.8	5.0	0.3	4.6	3.9	9.1	1.2	5.4	0.9	193.4	8.8
1007+417	*	82.0	2.6		4.7	0.1	154.3	0.2	1075.9	23.6	60.3	1.7		5.6	0.2	148.4	1.4	35.7	1.4	5.5	0.2	147.5	3.2	18.1	1.8	5.4	0.6	146.4	5.6
1014+392	*	7.0	1.7		0.5	0.1	97.8	2.4	855.6	18.1	22.7	1.5		2.7	0.2	161.5	3.3	20.2	0.7	3.9	0.1	137.8	3.3	25.4	1.8	11.1	0.8	149.9	3.7
1019+394		8.3	1.2		1.7	0.2	149.2	2.0	260.6	5.8	4.9	0.9		1.9	0.4	100.0	8.8	9.7	0.3	6.9	0.2	122.6	3.0	6.1	1.2	13.4	2.8	158.5	11.7
1020+400	*	71.6	2.6		6.3	0.2	121.0	0.2	1015.6	21.6	42.3	1.6		4.2	0.2	95.3	1.7	28.9	1.6	4.2	0.2	72.3	3.3	24.7	1.8	2.9	0.2	68.9	4.2
1022+432		23.3	1.8		2.7	0.2	98.7	0.7	449.5	10.2	30.0	1.0		6.7	0.3	85.8	1.6	15.0	0.4	6.7	0.2	72.0	3.1	10.2	2.0	13.4	2.6	101.0	10.5
1024+463	*	120.2	3.7		8.3	0.3	96.9	0.1	760.6	17.2	75.3	2.4		9.9	0.4	96.7	1.7	37.4	1.1	9.7	0.3	91.5	3.1	13.1	1.8	6.1	1.6	106.2	14.1
1025+390B	*	0.0	0.0	<	1.6	0.0	0.0	0.0	448.9	9.8	20.3	1.1		4.5	0.3	70.7	2.8	24.7	0.5	8.2	0.2	92.8	3.0	5.3	1.5	2.4	0.7	98.3	16.5
1030+415	*	13.6	1.4		2.8	0.3	86.6	1.2	419.4	11.6	5.3	1.3		1.3	0.3	64.7	13.1	18.0	0.4	6.6	0.2	72.2	3.0	3.9	1.3	1.7	0.6	55.6	16.8
1034+404	*	0.0	0.0	<	0.1	0.0	0.0	0.0	434.4	9.4	5.8	0.9		1.3	0.2	75.1	25.0	1.2	0.4	0.7	0.1	4.2	12.2	5.0	1.8	6.0	2.1	39.5	19.2
1044+454		0.0	0.0	<	0.0	0.0	0.0	0.0	195.3	4.7	0.0	0.0	<	2.3	0.0	0.0	0.0	3.3	0.3	3.8	0.3	87.9	4.6	3.5	1.4	14.8	5.7	195.4	23.2
1053+384		26.8	1.3		8.6	0.4	110.4	0.6	186.5	4.1	21.6	1.6		11.6	0.9	98.9	3.4	11.6	0.6	11.0	0.6	96.5	3.4	6.9	1.0	13.2	2.5	98.0	10.8
1053+394		13.4	1.1		11.3	0.9	66.5	1.2	68.4	2.1	9.0	0.8		13.2	1.3	48.2	6.4	0.0	0.0	0.0	0.0	0.0	3.0	3.0	1.0	18.3	6.5	34.5	17.0
1056+432A	*	120.4	3.0		4.1	0.1	67.7	0.1	1648.4	37.1	65.0	1.4		3.9	0.1	39.2	0.9	48.9	2.0	5.4	0.2	5.7	3.2	11.2	2.4	3.4	0.7	9.0	11.6
1101+384	*	13.3	1.8		1.5	0.2	112.0	1.2	819.1	18.2	12.9	1.1		1.6	0.1	141.4	5.6	33.8	0.7	5.0	0.1	113.5	3.0	22.4	1.8	4.3	0.4	126.9	4.3
1103+393		10.1	1.1		5.1	0.6	150.3	1.7	106.7	2.9	6.6	1.2		6.2	1.1	28.7	20.0	4.0	0.4	6.4	0.6	29.2	10.0	3.7	1.1	13.2	3.9	176.0	18.1
1105+392	*	58.1	2.6		6.5	0.3	42.4	0.3	488.3	11.0	30.5	1.6		6.2	0.3	40.2	2.5	20.7	0.6	7.5	0.3	41.5	3.1	12.3	2.1	9.6	1.7	38.2	9.4
1106+380	*	0.0	0.0	<	0.3	0.0	0.0	0.0	941.9	24.0	5.9	1.1		0.7	0.1	50.0	12.1	6.2	0.5	0.8	0.0	116.8	4.2	5.5	1.6	1.5	0.3	97.5	15.0
1107+379	*	65.1	2.6		2.9	0.1	0.5	0.3	1261.7	28.8	83.9	1.8		6.6	0.2	163.4	0.9	93.2	1.2	14.0	2.5	158.5	3.0	21.7	1.9	7.4	0.7	154.3	4.7
1108+399		8.4	1.2		2.2	0.3	11.4	2.0	213.9	5.1	4.3	1.0		2.0	0.5	185.6	13.3	10.1	0.2	6.8	0.2	160.5	3.0	3.2	0.5	4.0	0.7	170.4	9.1
1109+437	*	35.9	1.7		2.5	0.1	62.7	0.5	762.2	17.0	27.0	1.0		3.5	0.2	60.0	2.0	17.2	0.5	5.1	0.2	54.1	3.1	6.2	1.5	4.3	1.1	56.8	13.1
1111+408	*	46.5	2.3		1.5	0.1	74.8	0.4	1467.5	31.4	35.2	1.4		2.4	0.1	84.3	1.8	19.6	0.5	2.6	0.1	105.3	3.1	19.4	1.9	7.8	0.8	119.8	5.1

Table 3. continued.

Name		1.4 GHz						2.7 GHz								4.8 GHz						10.5 GHz					
		S_p	ΔS_p		m	Δm	χ	$\Delta\chi$	S	ΔS	S_p	ΔS_p		m	Δm	χ	$\Delta\chi$	S_p	ΔS_p		m	Δm	χ	$\Delta\chi$	S_p	ΔS_p	m	Δm	χ	$\Delta\chi$
		[mJy]			[%]		[°]		[mJy]		[mJy]			[%]		[°]		[mJy]			[%]		[°]		[mJy]		[%]		[°]	
1112+435		22.4	1.7		6.5	0.5	71.2	0.7	206.3	4.9	16.2	1.2		7.8	0.6	179.0	3.5	10.9	0.4		8.5	0.3	170.2	3.2	8.5	1.8	13.4	2.8	166.6	10.3
1122+390		20.1	1.7		15.1	1.3	129.0	0.8	85.1	2.8	12.3	0.9		14.5	1.1	126.4	4.4	6.7	0.4		12.9	0.6	128.1	3.4	2.8	0.4	7.8	1.2	127.0	7.9
1128+385	*	5.5	1.3		0.8	0.2	154.6	3.0	733.1	16.1	10.0	0.9		1.4	0.1	2.9	4.6	7.2	0.7		1.1	0.1	10.3	3.8	17.9	1.7	1.9	0.2	53.1	4.5
1131+391		0.0	0.0	<	1.6	0.0	0.0	0.0	107.9	3.0	0.0	0.0	<	3.4	0.0	0.0	0.0	1.4	0.0	<	1.4	0.0	0.0	3.0	16.6	1.6	22.3	2.3	84.6	5.0
1131+437	*	28.1	1.7		1.7	0.1	31.7	0.6	890.1	20.2	30.5	1.0		3.4	0.1	149.9	1.7	7.3	0.4		1.4	0.1	84.9	3.6	6.3	1.9	2.9	0.9	74.8	15.2
1141+392		10.8	1.2		5.0	0.6	178.5	1.5	112.4	3.5	0.0	0.0	<	4.4	0.0	0.0	0.0	3.7	0.3		5.8	0.9	158.7	4.4	3.0	0.9	10.3	3.0	143.7	17.9
1141+466		0.0	0.0	<	0.1	0.0	0.0	0.0	423.8	10.5	0.0	0.0	<	0.9	0.0	0.0	0.0	2.5	0.4		1.2	0.1	10.8	7.0	2.6	0.9	4.3	1.5	112.0	23.3
1148+387	*	32.7	1.3		4.9	0.2	152.6	0.5	349.6	7.5	27.9	1.0		8.0	0.3	124.6	2.0	21.4	0.6		9.4	0.3	119.0	3.1	12.5	1.7	9.0	1.2	111.5	7.7
1151+383		9.8	1.4		1.8	0.3	168.8	1.7	295.3	7.0	12.9	1.3		4.4	0.5	21.0	5.3	7.0	0.4		4.2	0.4	7.7	3.8	5.6	1.5	8.3	2.2	42.2	14.7
1151+408	*	17.2	1.3		1.5	0.1	111.5	1.0	625.1	13.2	17.2	1.1		2.8	0.2	88.0	3.0	24.5	0.8		4.9	0.2	83.5	3.1	34.1	1.3	8.6	0.4	93.5	2.2
1151+456	*	8.3	1.5		0.8	0.2	32.3	2.0	582.3	12.7	6.9	0.9		1.2	0.2	25.2	7.0	7.1	0.5		2.0	0.1	4.2	4.5	4.7	1.4	2.3	0.7	197.9	14.5
1153+451	*	29.3	1.8		3.9	0.2	5.6	0.6	399.1	8.9	14.9	0.9		3.7	0.2	21.7	3.3	10.0	0.4		4.4	0.2	21.6	3.3	5.2	1.7	4.9	1.8	26.8	16.3
1206+439B	*	161.6	5.0		8.0	0.2	41.4	0.1	1104.5	23.5	87.6	2.0		7.9	0.2	39.6	0.6	61.4	1.4		10.2	0.3	41.9	3.0	32.8	3.0	12.5	1.2	39.9	4.2
1209+396		8.2	1.1		3.0	0.4	118.6	2.0	144.8	3.3	11.8	1.0		8.1	0.7	117.4	4.9	5.2	0.3		6.9	0.3	95.2	3.6	4.4	1.3	13.8	4.3	175.7	20.1
1220+393		7.7	1.2		7.5	1.2	171.7	2.2	54.1	1.7	3.8	1.0		7.0	1.9	177.4	15.8	2.6	0.3		9.8	0.9	19.0	4.9	3.5	0.9	29.9	9.7	0.4	13.3
1220+408		0.0	0.0	<	0.3	0.0	0.0	0.0	223.4	6.6	3.9	1.0		1.7	0.5	85.7	13.2	6.7	0.5		6.1	0.3	60.0	3.8	4.5	0.4	9.5	0.9	53.4	5.1
1222+423	*	62.1	2.1		4.5	0.2	106.8	0.3	706.9	16.6	67.6	1.6		9.6	0.3	117.8	1.0	29.3	0.9		8.0	0.3	112.6	3.2	8.6	1.0	5.8	0.7	103.1	7.5
1223+395	*	0.0	0.0	<	0.2	0.0	0.0	0.0	572.9	12.6	9.3	0.8		1.6	0.2	130.1	4.9	4.9	0.3		1.0	0.1	12.8	4.5	4.6	0.8	1.5	0.3	144.0	13.4
1232+414A	*	47.4	1.7		6.4	0.2	27.5	0.4	427.1	9.8	33.0	1.5		7.7	0.4	43.9	2.3	14.2	0.5		6.0	0.2	45.7	3.3	6.7	1.0	7.2	1.1	53.7	9.0
1233+418	*	0.0	0.0	<	0.6	0.0	0.0	0.0	422.3	9.4	0.0	0.0	<	1.4	0.0	0.0	0.0	11.1	0.5		4.2	0.2	162.9	3.4	6.9	1.6	5.3	1.3	166.9	12.7
1234+396	*	23.3	1.5		6.6	0.4	131.5	0.7	287.2	6.3	19.6	1.0		6.8	0.4	157.7	2.6	16.8	0.5		7.2	0.3	166.8	3.2	8.2	1.2	4.8	0.7	170.6	8.8
1239+442B	*	50.9	2.0		10.1	0.4	98.3	0.3	280.8	8.9	31.7	1.4		11.3	0.6	68.1	2.2	12.8	0.5		7.5	1.1	66.3	3.3	8.8	1.8	9.7	2.5	61.0	11.7
1240+381	*	9.0	1.3		1.6	0.2	19.4	1.8	555.9	11.9	10.4	0.9		1.9	0.2	157.0	5.0	13.5	0.5		1.9	0.1	177.9	3.2	4.8	1.7	1.5	0.5	187.5	16.7
1247+450A	*	33.8	1.8		4.9	0.3	162.7	0.5	374.0	9.1	23.1	1.1		6.2	0.3	149.1	2.6	18.4	0.4		8.5	0.3	149.0	3.0	8.1	2.1	8.4	2.3	165.1	14.1
1249+432		17.6	1.6		3.1	0.3	100.2	0.9	282.7	8.5	13.4	1.3		4.7	0.5	173.4	5.8	11.0	0.5		6.5	1.0	129.7	3.4	6.5	1.0	9.4	1.5	102.9	9.8
1249+475	*	40.1	2.2		4.1	0.2	49.6	0.4	341.5	7.5	27.0	1.0		7.9	0.3	6.6	1.7	28.5	0.7		12.5	0.4	169.7	3.1	7.1	1.3	8.0	1.8	156.8	12.8
1253+432		0.0	0.0	<	0.4	0.0	0.0	0.0	219.0	5.3	0.0	0.0	<	3.4	0.0	0.0	0.0	1.2	0.3		1.0	0.2	14.2	11.1	4.7	1.8	8.0	3.1	57.8	17.4
1254+476	*	84.3	2.9		1.6	0.1	7.6	0.2	2901.2	62.7	135.1	2.9		4.7	0.1	30.9	0.5	112.2	2.3		6.7	0.2	41.8	3.0	84.3	2.7	11.6	0.4	50.9	1.5
1258+395		8.4	1.1		12.5	1.7	158.6	2.0	35.2	1.3	6.2	0.9		17.5	2.7	156.0	8.4	2.9	0.3		14.0	1.1	156.3	4.2	2.3	0.5	19.0	6.2	140.3	16.1
1258+404	*	21.9	2.0		1.6	0.1	170.1	0.8	694.7	15.9	17.1	1.0		2.5	0.2	3.8	2.8	19.5	0.9		5.5	0.2	21.7	3.4	13.2	1.3	9.4	1.0	26.8	5.3
1301+382		30.2	1.7		5.2	0.3	168.2	0.5	310.9	9.5	18.3	1.1		5.9	0.4	158.0	3.4	12.1	0.4		6.6	0.2	158.7	3.2	7.2	2.1	9.0	2.8	137.9	13.6
1308+392		8.5	1.1		4.8	0.6	150.4	1.9	114.1	2.9	8.3	0.9		7.3	0.8	170.2	6.2	7.0	0.3		9.2	0.4	10.8	3.4	9.6	1.3	26.4	3.6	169.4	6.5
1312+393		5.7	1.3		2.2	0.5	94.7	2.9	143.1	3.4	6.2	1.0		4.3	0.7	79.8	8.3	3.6	0.4		4.3	0.3	93.5	4.5	4.1	0.7	10.3	1.8	49.9	12.2
1315+395		0.0	0.0	<	1.3	0.0	0.0	0.0	126.5	4.0	4.4	1.0		3.5	0.8	169.8	11.1	4.9	0.4		6.3	0.5	176.3	4.7	7.0	1.7	22.7	5.6	4.2	12.0
1315+396	*	16.9	2.1		2.6	0.3	50.9	1.0	437.6	9.4	18.6	1.0		4.3	0.2	49.7	2.9	18.6	0.7		5.1	0.3	43.8	3.3	6.0	1.6	2.1	0.6	189.4	13.4
1317+380		0.0	0.0	<	0.9	0.0	0.0	0.0	155.8	4.1	5.8	1.0		3.7	0.6	96.4	8.9	5.2	0.4		5.1	0.6	95.7	4.8	5.0	0.8	10.7	1.8	97.3	10.5
1321+415	*	37.3	1.4		5.9	0.2	116.5	0.4	350.7	7.9	26.4	0.9		7.5	0.3	126.0	1.8	14.3	0.5		6.8	0.3	126.9	3.8	9.3	2.1	10.5	2.3	133.9	12.0
1333+412	*	0.0	0.0	<	0.4	0.0	0.0	0.0	446.0	9.5	5.0	0.7		1.1	0.2	122.7	9.2	3.6	0.3		1.4	0.1	145.6	4.5	6.0	2.0	6.3	2.2	43.8	17.3
1336+391A	*	0.0	0.0	<	0.1	0.0	0.0	0.0	1765.6	38.0	7.3	0.9		0.7	0.1	49.5	6.7	29.7	0.6		3.1	0.1	21.1	3.0	21.8	2.1	6.0	0.6	11.8	4.8
1339+472	*	40.2	1.6		5.6	0.2	124.9	0.4	379.7	8.5	26.0	1.2		6.9	0.4	64.8	2.3	19.2	0.4		9.0	0.3	45.9	3.1	6.5	1.6	7.6	1.9	31.9	11.1

Table 3. continued.

name		1.4 GHz							2.7 GHz								4.8 GHz						10.5 GHz					
		S_p	ΔS_p		m	Δm	χ	$\Delta\chi$	S	ΔS	S_p	ΔS_p		m	Δm	χ	$\Delta\chi$	S_p	ΔS_p	m	Δm	χ	$\Delta\chi$	S_p	ΔS_p	m	Δm	χ	$\Delta\chi$
		[mJy]			[%]		[°]		[mJy]		[mJy]			[%]		[°]		[mJy]		[%]		[°]		[mJy]		[%]		[°]	
1343+386	*	0.0	0.0	<	0.3	0.0	0.0	0.0	581.2	12.6	5.4	0.9		0.9	0.2	108.7	9.0	11.5	0.4	2.9	0.1	94.4	3.2	5.5	1.3	2.8	0.7	98.2	16.8
1343+430	*	7.7	1.3		0.7	0.1	63.8	2.2	678.2	14.5	10.2	1.0		1.5	0.2	164.9	5.1	9.3	0.6	2.3	0.1	130.1	3.6	5.8	1.1	3.6	0.7	130.9	13.6
1347+403		7.0	1.1		5.1	0.8	137.6	2.4	61.7	2.2	7.3	0.9		11.8	1.6	139.5	7.5	5.4	0.3	15.3	0.9	140.4	3.7	3.2	0.5	24.8	4.3	145.2	8.1
1349+388	*	0.0	0.0	<	1.3	0.0	0.0	0.0	204.8	4.6	7.0	1.0		3.4	0.5	156.2	8.2	4.4	0.3	2.7	0.2	151.0	3.7	3.9	0.7	3.4	0.6	127.3	10.4
1354+397		4.9	1.3		2.2	0.6	97.3	3.4	88.1	3.1	4.5	1.3		5.1	1.5	137.1	15.9	4.5	0.4	13.0	1.4	140.0	4.3	1.9	0.7	16.2	5.6	134.5	20.4
1408+398		4.5	1.3		2.9	0.8	24.8	3.7	82.7	2.8	0.0	0.0	<	4.5	0.0	0.0	0.0	0.9	0.3	1.9	0.5	10.7	13.5	10.4	1.0	64.6	7.8	80.8	6.1
1416+400		4.4	1.1		1.7	0.4	117.5	3.7	157.1	5.8	0.0	0.0	<	3.5	0.0	0.0	0.0	1.5	0.3	1.3	0.2	126.8	8.1	7.6	1.0	10.3	1.5	136.9	10.9
1417+385	*	12.2	1.2		2.0	0.2	91.4	1.4	891.1	19.3	19.6	0.9		2.2	0.1	110.4	2.5	31.5	0.6	2.3	0.1	152.3	3.1	9.0	1.7	1.5	0.2	35.1	10.9
1419+397	*	0.0	0.0	<	0.0	0.0	0.0	0.0	271.3	6.1	0.0	0.0	<	1.8	0.0	0.0	0.0	2.2	0.2	1.2	0.1	119.3	3.0	3.8	1.3	3.9	1.4	78.7	20.0
1432+382		11.1	1.2		2.4	0.3	99.1	1.5	323.0	7.1	7.3	1.0		2.3	0.3	81.5	7.5	3.7	0.2	2.2	0.1	83.3	3.0	3.4	1.2	4.7	1.7	48.2	18.3
1435+429		9.4	1.2		3.4	0.4	166.2	1.8	158.9	4.4	8.1	1.1		5.1	0.7	23.6	7.1	10.5	0.4	9.8	0.5	20.6	3.6	3.5	0.9	13.4	3.3	194.1	16.5
1438+385	*	36.0	1.6		3.3	0.1	123.9	0.5	966.5	20.3	37.9	1.0		3.9	0.1	129.3	1.3	19.7	0.8	2.5	0.1	122.2	3.2	21.8	2.0	3.4	0.3	127.6	4.5
1445+410	*	7.8	1.3		1.8	0.3	88.5	2.1	251.0	6.1	10.2	1.1		4.1	0.5	116.1	6.2	5.8	0.4	3.5	0.2	138.0	4.0	5.1	1.2	5.0	1.2	131.9	16.1
1446+440		12.2	1.3		2.3	0.2	68.9	1.4	286.1	6.7	6.0	1.0		2.1	0.4	118.2	9.5	2.9	0.3	1.9	0.2	77.9	5.4	5.6	0.9	8.0	1.4	72.6	12.3
1450+396		5.1	1.1		9.9	2.1	34.6	3.3	26.2	1.7	4.3	0.9		16.4	3.6	47.8	12.0	6.0	0.2	33.2	1.3	49.0	3.0	1.1	0.4	14.9	6.5	188.7	17.8
1455+421	*	10.4	1.4		2.0	0.3	35.4	1.6	314.6	6.9	9.6	0.9		3.1	0.3	31.3	5.7	10.8	0.4	5.3	0.2	51.0	3.3	7.8	1.4	6.8	1.2	55.2	9.4
2304+377	*	6.0	1.6		0.4	0.1	69.0	2.8	918.5	19.5	10.1	0.9		1.1	0.1	53.9	4.8	4.7	1.2	0.9	0.1	16.0	10.4	7.7	1.1	3.3	0.5	174.7	11.0
2308+400		0.0	0.0	<	1.5	0.0	0.0	0.0	91.6	2.7	7.3	0.8		7.9	0.9	66.6	5.5	5.0	0.4	10.2	0.7	84.8	4.1	2.6	0.5	15.4	3.2	100.1	10.8
2313+406		19.2	1.4		8.5	0.6	175.8	0.9	119.4	5.5	9.5	0.6		8.0	0.7	53.7	4.5	6.1	0.3	9.2	0.5	73.3	3.6	5.1	1.9	20.0	7.8	83.0	17.3
2322+396	*	3.6	1.1		3.2	0.9	123.0	4.6	73.7	2.9	0.0	0.0	<	3.9	0.0	0.0	0.0	2.1	0.3	2.2	0.3	109.4	7.3	5.0	1.3	4.3	1.1	98.4	16.5
2323+388		5.8	1.2		3.0	0.6	43.7	2.8	113.4	3.1	5.9	0.7		5.2	0.7	139.5	9.7	3.2	0.4	4.8	0.5	158.4	5.2	1.5	0.7	4.9	2.1	142.9	18.7
2324+405	*	67.8	2.3		2.8	0.1	117.0	0.2	1571.4	37.5	50.3	1.3		3.2	0.1	176.7	1.1	30.5	1.0	3.1	0.2	10.1	3.1	19.0	1.6	4.3	0.4	18.5	4.7
2326+422	*	49.0	2.0		10.9	0.4	81.6	0.3	289.1	13.3	35.9	1.1		12.4	0.7	81.8	1.6	20.6	0.4	11.7	0.3	85.7	3.0	14.4	2.0	15.0	2.1	82.0	8.1
2327+391		0.0	0.0	<	1.4	0.0	0.0	0.0	56.4	2.7	4.2	1.0		7.4	1.8	34.8	13.1	1.7	0.3	5.2	0.8	49.4	8.4	1.7	0.5	11.8	3.9	53.5	16.0
2332+388		3.3	1.1		2.4	0.8	148.7	5.0	73.4	2.4	6.6	0.7		9.0	1.0	98.8	5.2	6.0	0.4	13.1	0.8	129.6	3.9	2.9	0.5	15.3	2.8	146.6	9.8
2338+390		0.0	0.0	<	1.6	0.0	0.0	0.0	127.8	2.9	6.7	0.8		5.2	0.6	129.5	6.8	5.1	0.3	6.4	0.4	149.3	3.7	2.3	0.5	5.7	1.3	169.3	14.3
2341+396A		0.0	0.0	<	1.1	0.0	0.0	0.0	111.5	2.6	3.5	0.7		3.1	0.6	145.4	12.3	5.7	0.4	10.6	0.6	138.7	4.1	2.5	0.3	12.3	1.5	141.1	6.9
2344+429	*	0.0	0.0	<	0.4	0.0	0.0	0.0	420.1	9.5	6.0	0.7		1.4	0.2	138.6	8.6	11.4	0.2	4.0	0.1	133.0	3.0	5.1	1.0	2.0	0.4	64.8	11.0
2350+395	*	0.0	0.0	<	1.6	0.0	0.0	0.0	187.8	4.3	7.0	0.9		3.7	0.5	114.4	7.3	5.1	0.2	2.6	0.1	169.1	3.0	10.0	0.8	3.8	0.3	160.7	3.9
2351+456	*	0.0	0.0	<	0.1	0.0	0.0	0.0	1759.4	37.7	10.3	1.1		0.7	0.1	150.1	6.1	17.9	0.4	1.4	0.0	103.4	3.0	22.5	1.6	3.1	0.2	79.8	3.7
2356+390	*	7.0	1.4		1.6	0.3	100.1	2.4	318.8	8.4	0.0	0.0	<	1.0	0.0	0.0	0.0	5.2	0.2	2.0	0.1	166.9	3.0	6.8	1.0	2.8	0.4	45.4	10.1
2356+437	*	134.0	3.3		6.7	0.2	74.0	0.1	1028.9	23.2	105.3	2.1		10.2	0.3	111.2	0.6	56.9	0.9	12.0	0.3	126.1	3.0	22.7	1.2	12.2	0.7	126.7	2.8
2358+406	*	0.0	0.0	<	0.1	0.0	0.0	0.0	858.2	18.3	7.3	0.9		0.9	0.1	75.9	6.6	3.6	0.2	0.7	0.0	148.6	3.0	4.2	1.2	1.6	0.5	37.3	17.8

as the slope of the linear relation

$$\Delta\chi = RM \cdot \lambda^2.$$

Here, n_e is the number density of thermal electrons, $B_{||}$ the strength of the magnetic field component along the line-of-sight, and s_0 the effective path length. With three or more well spaced frequencies it is possible to remove the $n \cdot \pi$ ambiguity. In the polarized sample we have 143 sources with χ measured at four wavelengths and 26 sources with χ measured at only three wavelengths. The method we used to obtain *RM* is the following:

a) a visual inspection of the plot of χ vs. λ^2 permitted us to verify the linearity of the relation taking into account the errors of χ;

b) when needed (for 90% of sources) we added the minimum number of $\pm n \cdot \pi$ to the angles corresponding to the longest wavelengths, such as to have an approximately linear relation;

c) run a least-square fit to the data.

For a minority of sources (see Saikia & Salter 1988 for a review) some deviation from linearity can be present at longer wavelengths in the relation between χ and λ^2. Therefore, we excluded the values of χ at 1.4 GHz for 29 sources which show a χ^2 greater than 3 and repeated the least-square fit, obtaining a reliable measure of *RM*. Finally, we obtained a fit to the data with a χ^2 less than 3 for a total of 143 sources, allowing a reliable determination of *RM*. For the remaining sources the data could not be fitted; this behaviour may be due to variability and, in fact, the majority of these sources have flat spectra.

Table 4 presents the source name in Col. 1 and the redshift in Col. 2 (negative value means that redshift has been estimated from magnitudes; a blank cell means that no redshift is available and that a redshift of 1.1 could be used (median value for the B3-VLA sample); Galactic latitude and longitude coordinates are given in Cols. 3 and 4, and the Rotation Measure and its error in Cols. 5 and 6. The spectral index between 408 MHz and 10.5 GHz is listed in Col. 7. We have computed the median absolute *RM*s (and errors) for sources with $|b_{II}| > 40^\circ$ (69 objects), resulting in $RM = 8^{+2}_{-5}$ rad m^{-2}, while for sources with $|b_{II}| \leq 25^\circ$ (54 objects) we obtain $RM = -68^{+13}_{-6}$ rad m^{-2}.

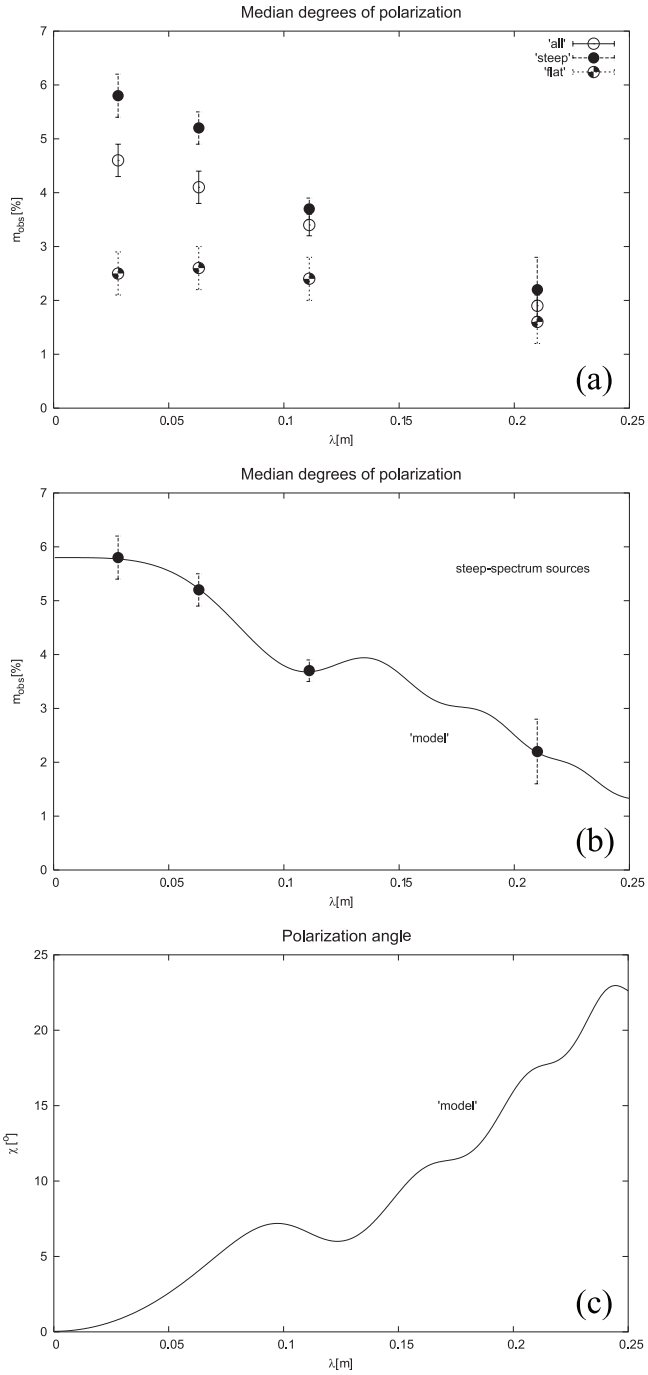

Fig. 2. a) Median degrees of polarisation m_{obs} plotted versus wavelength. Open circles represent all sources of the "complete sample", while filled circles and those with diamonds represent steep- and flat-spectrum sources, respectively. **b)** Median m_{obs}, with a three-component "model" (see text) superimposed. **c)** Source-intrinsic Faraday rotation as resulting from the "model".

4.3. Depolarisation

4.3.1. Median polarisation

The median degrees of polarisation of the "complete sample" at all four frequencies are plotted in Fig. 2a. The steep-spectrum sources show a decrease of the degree of polarisation, which does not drop to zero towards lower frequencies. The flat-spectrum sample exhibits a largely constant degree of linear polarisation, as is to be expected (see also Saikia & Salter 1988).

The overall degrees of polarisation at all four wavelengths are obviously degraded by beam depolarisation, since we report solely integrated values here. The maximum degree of polarisation expected for a source depends on the spectral index. Without any depolarisation effects, one would then expect a theoretical value

$$P_0 = \frac{3 - 3 \cdot \alpha}{5 - 3 \cdot \alpha}$$

where α is the spectral index ($S \propto \nu^\alpha$) and the subscript "0" refers to zero wavelength (where there are no Faraday effects). The mean spectral index of our steep-spectrum sample

Table 4. Rotation Measures based on measurements at four different frequencies.

Name	redshift	$l_{\rm II}$ [$\circ$]	$b_{\rm II}$ [$\circ$]	*RM* [rad/m^2]	error [rad/m^2]	$\alpha_{408\ \rm MHz}^{10.6\ \rm GHz}$	Name	redshift	$l_{\rm II}$ [$\circ$]	$b_{\rm II}$ [$\circ$]	*RM* [rad/m^2]	error [rad/m^2]	$\alpha_{408\ \rm MHz}^{10.6\ \rm GHz}$
0010+405	0.2550	115.2	−21.4	−87.0	4.8	−0.44	0800+472		172.3	31.5	−23.1	6.3	−0.78
0013+387	1.7210	115.4	−23.3	−123.9	4.0	−0.90	0805+406		180.0	31.4	25.8	3.1	−0.78
0022+390	1.9320	117.5	−23.3	−99.6	2.0	−0.26	0806+426	1.1840	177.9	31.9	−405.6	7.3	−1.08
0029+394	0.9274	119.0	−23.0	−99.6	0.8	−0.97	0809+404	0.5510	180.5	32.1	−164.9	15.9	−0.78
0032+423	1.5880	119.7	−20.1	105.8	16.7	−0.85	0811+388	0.1320	182.5	32.2	14.8	2.3	−1.05
0041+382A		121.3	−24.3	−108.8	3.4	−1.12	0818+472A	0.1300	172.7	34.5	−16.1	2.1	−0.99
0041+393		121.4	−23.2	−99.2	4.2	−0.81	0820+431	−.4500	177.7	34.4	−0.9	2.1	−1.06
0045+404		122.4	−22.1	−81.1	1.6	−0.93	0821+447	0.8930	175.7	34.9	31.5	8.8	−0.98
0051+404	−1.380	123.5	−22.2	−131.0	4.6	−0.96	0827+378	0.9140	184.3	35.1	191.2	2.3	−0.74
0052+395		123.8	−23.1	−71.7	6.1	−0.77	0836+426	0.5950	178.7	37.4	6.0	6.9	−0.53
0057+395		124.7	−23.0	−96.2	2.5	−0.80	0841+403	0.5272	181.7	38.1	11.7	2.9	−0.94
0059+461		125.0	−16.4	−88.2	5.1	−1.11	0849+424	0.9780	179.1	39.7	284.6	4.8	−0.98
0105+441	−1.363	126.1	−18.4	−70.6	3.8	−0.84	0852+384		184.4	40.1	15.5	2.2	−0.90
0109+416B	−.1800	127.1	−20.8	−149.3	4.3	−1.09	0854+399B	0.5280	182.4	40.5	19.2	2.9	−0.94
0110+401	1.4790	127.4	−22.2	−64.2	1.5	−0.63	0857+391	0.2280	183.6	41.1	19.3	3.0	−0.84
0113+400		128.1	−22.3	−114.8	1.1	−0.93	0858+452		175.5	41.5	35.9	2.8	−0.95
0115+453A	1.3010	127.8	−17.0	−51.7	4.2	−1.05	0900+428	−.3300	178.7	41.9	16.9	2.2	−0.56
0116+438	−.2200	128.2	−18.5	−47.6	0.9	−0.84	0904+417B	−.2800	180.1	42.5	43.4	3.0	−0.94
0130+381	−.3900	132.0	−23.7	−9.1	3.6	−0.73	0905+380A	0.8970	185.2	42.6	−10.0	2.8	−1.18
0133+381		132.6	−23.6	−40.6	11.1	−0.96	0906+383		184.9	42.8	14.0	3.2	−1.06
0139+389A	1.1060	133.6	−22.6	−84.1	5.0	−0.73	0911+418	0.1400	180.1	43.8	−9.4	1.8	−0.68
0149+398	0.0790	135.3	−21.3	−78.2	5.0	−0.63	0913+385	0.0710	184.7	44.1	14.4	2.5	−0.75
0152+435	0.8270	135.0	−17.6	−45.9	5.0	−0.95	0913+391	1.2500	183.8	44.2	1.9	1.6	−0.39
0153+417	0.4880	135.6	−19.2	−73.1	3.1	−0.95	0918+381	1.1080	185.3	45.1	16.7	9.7	−0.96
0157+442	0.7210	135.7	−16.7	−113.3	3.5	−0.96	0922+422	1.7500	179.4	45.9	−11.5	36.0	−1.19
0202+380	−.2500	138.7	−22.3	−74.9	5.3	−0.81	0937+391	0.6180	183.9	48.9	−6.0	3.9	−0.90
0213+392	0.9630	140.3	−20.5	−74.8	5.6	−0.97	0955+390		183.7	52.3	−12.4	7.9	−0.90
0213+412	0.5150	139.6	−18.6	162.0	35.4	−0.75	1004+446		174.1	53.0	26.5	4.4	−1.00
0216+423		139.7	−17.4	−84.2	5.4	−0.93	1007+417	0.6130	178.6	54.2	3.0	0.2	−0.78
0218+396		141.2	−19.7	−82.0	2.4	−0.91	1019+394	0.9230	182.1	56.9	−69.2	5.8	−1.07
0219+428A	0.4440	140.1	−16.8	−166.0	4.2	−0.45	1020+400	1.2500	180.9	56.9	40.8	4.0	−0.24
0220+393A	−.2200	141.6	−19.9	−94.2	5.6	−0.57	1022+432	−1.496	175.1	56.6	−299.3	10.0	−1.11
0220+397	1.1760	141.5	−19.5	−85.7	0.9	−1.07	1024+463	0.5250	169.6	55.9	−8.6	3.6	−0.92
0224+396		142.4	−19.4	−101.3	5.0	−0.86	1025+390B	0.3610	182.4	58.1	−41.7	3.3	−0.61
0243+439		143.7	−14.0	−55.1	3.5	−0.79	1030+415	1.1200	177.4	58.4	9.6	3.9	−0.47
0246+392		146.5	−17.9	−41.6	3.9	−0.79	1034+404	0.8270	179.0	59.4	−215.0	6.2	−1.01
0247+404	0.6510	146.2	−16.7	−66.7	1.5	−0.94	1053+384		181.1	63.5	5.3	0.7	−0.83
0250+384		147.7	−18.2	−41.3	3.7	−1.24	1053+394		178.8	63.3	12.0	2.4	−0.88
0251+393	0.2910	147.4	−17.4	−49.4	3.8	0.11	1056+432A	0.7480	170.7	62.3	49.8	5.7	−0.95
0258+443		146.1	−12.4	−59.6	1.8	−0.86	1103+393		177.6	65.0	56.4	7.2	−0.91
0710+457	−.1700	171.9	22.9	3.1	2.5	−0.78	1105+392	0.7810	177.4	65.5	1.1	0.8	−0.90
0723+397		178.9	23.4	21.1	7.5	−0.91	1107+379	0.3460	180.3	66.2	9.6	0.8	−0.92
0736+400	−.1900	179.4	25.9	2.0	0.6	−0.82	1108+399	0.5900	175.4	65.8	9.5	5.1	−0.77
0739+397B	1.7000	179.8	26.4	8.7	4.6	−0.45	1109+437	1.6800	167.2	64.2	2.7	1.2	−1.09
0739+398	2.1860	179.7	26.3	5.6	7.0	−0.19	1111+408	0.7340	172.6	65.9	−50.4	6.5	−1.18
0742+394		180.4	26.8	−1.0	3.6	−1.10	1112+435	−.2500	167.0	64.8	33.5	2.4	−0.80
0743+392B		180.6	27.0	30.2	2.8	−1.08	1122+390	0.0070	174.7	68.5	0.7	0.5	−0.57
0751+392		181.0	28.4	15.5	0.8	−0.89	1131+437	0.5720	161.5	67.5	124.9	2.9	−0.90
0754+396	2.1190	180.8	29.1	4.9	1.4	−1.07	1148+387	1.3030	167.2	73.1	15.5	1.2	−0.81
0756+377		182.9	29.0	32.1	3.7	−1.02	1151+456	0.1920	151.1	68.5	7.8	4.6	−0.76

is $\alpha = -0.92$, for which in the absence of beam depolarisation we would hence expect a maximum degree of polarisation of ∼74%. Figure 2a shows that this is strongly degraded already at 10.5 GHz, viz. by a factor of ∼15. If the magnetic field has an isotropic random component within the telescope beam size, this gives rise to a *frequency-independent* depolarisation of the form (Burn 1966)

$$m_0 = P_0 \cdot \frac{B_{\rm u}^2}{B_{\rm u}^2 + B_{\rm r}^2}.$$

Table 4. continued.

Name	redshift	$l_{\rm II}$ [°]	$b_{\rm II}$	*RM* [rad/m^2]	error	$\alpha_{408\ \rm MHz}^{10.6\ \rm GHz}$	Name	redshift	$l_{\rm II}$ [°]	$b_{\rm II}$	*RM* [rad/m^2]	error	$\alpha_{408\ \rm MHz}^{10.6\ \rm GHz}$
1153+451		151.3	69.1	−7.7	1.1	−0.88	1343+386	1.8440	81.1	74.0	18.5	11.0	−0.65
1206+439B	1.4000	147.5	71.4	0.3	0.6	−0.96	1343+430	1.0280	91.4	70.8	44.9	3.4	−0.88
1209+396		154.0	75.3	−368.0	4.6	−0.97	1347+403		83.7	72.3	−2.1	1.3	−1.09
1220+393		147.3	76.7	280.7	8.0	−1.00	1354+397		79.6	71.7	−16.2	3.3	−1.37
1220+408		144.9	75.3	48.8	3.6	−1.08	1435+429	−3.753	75.9	63.5	12.3	8.1	−1.11
1222+423	0.9440	141.4	74.0	19.3	3.8	−1.03	1438+385	1.7750	66.0	64.6	−0.7	1.9	−0.14
1232+414A	−.1700	135.8	75.5	−9.0	1.6	−0.93	1445+410	−.1800	70.3	62.6	−18.1	3.4	−0.71
1234+396		136.0	77.4	−14.8	0.8	−0.37	1446+440	−.7680	76.1	61.1	69.4	2.0	−0.94
1239+442B	0.6100	128.6	73.1	14.1	1.2	−0.81	1455+421	0.8750	71.2	60.3	−6.4	5.3	−0.78
1240+381	1.3160	131.9	79.1	−66.0	3.3	−0.07	2304+377	−.4000	101.2	−20.4	98.1	2.1	−0.75
1249+432	0.3900	122.5	74.2	100.9	7.1	−0.94	2308+400		103.0	−18.6	−46.8	10.4	−1.12
1249+475		122.5	69.9	41.9	3.2	−1.12	2313+406		104.2	−18.5	−32.9	2.0	−1.02
1254+476	0.9970	120.2	69.8	−27.9	2.5	−0.92	2323+388		105.3	−20.8	−43.2	6.8	−0.85
1258+395		114.5	77.7	4.2	4.1	−0.84	2324+405		106.1	−19.3	−31.0	0.7	−0.79
1258+404	1.6560	115.3	76.8	−34.6	3.8	−1.08	2326+422	0.2700	107.1	−17.8	−0.8	1.0	−0.74
1301+382	0.1260	110.3	78.9	8.1	5.0	−0.94	2327+391	3.0860	106.3	−20.8	−28.1	1.6	−1.00
1315+395		100.2	76.7	−19.5	6.7	−0.97	2332+388	3.2000	107.1	−21.4	−68.0	1.3	−0.96
1317+380	0.8350	95.4	77.8	−0.7	2.3	−0.87	2338+390	0.8160	108.4	−21.6	−54.8	15.4	−0.85
1321+415	−.3900	100.0	74.4	−5.6	1.5	−0.93	2341+396A	−.2000	109.2	−21.2	7.9	5.9	−0.91
1333+412	0.1870	92.7	73.4	657.3	28.1	−1.07	2351+456	2.0000	112.7	−15.8	102.0	7.6	−0.36
1336+391A	0.2460	85.7	74.7	56.2	1.5	−1.03	2356+437	1.6530	113.0	−17.8	−24.6	1.3	−1.05
1339+472	0.5020	99.7	67.8	46.4	2.7	−1.01							

This is nothing but the ratio of the energy in the uniform ($B_{\rm u}$) to that in the random ($B_{\rm r}$) magnetic field of the synchrotron-emitting source. Note that the polarisation measurements reported here deliver *integrated fluxes* for all Stokes parameters I, Q and U. In case of the NVSS data this was done via integrating the corresponding maps over the sources (most of which were point-like even for the $45''$ beam), while the single-dish measurements involved beam sizes larger than the source size anyhow. Also here, some of the sources with larger angular extents had been mapped, in which case integrated I, Q and U flux densities have been used to determine the polarisation properties.

In case of strong Faraday rotation, the measured degree of polarisation $m_{\rm obs}$ may be degraded due to bandwidth depolarisation (differential rotation of the polarisation angle across the band, see e.g., Gardner & Whiteoak 1966):

$$m_{\rm obs} = m_0 \cdot \frac{\sin\Delta\psi}{\Delta\psi},$$

where m_0 is the "monochromatic" degree of polarization and

$$\Delta\psi = -2 \cdot RM \cdot \lambda^2 \cdot \frac{\Delta\nu}{\nu_0},$$

is the total rotation across the band, and $\Delta\nu$ and ν_0 the bandwidth and centre frequency, respectively. The NVSS observations from which we have extracted the Stokes I, U and Q maps had been carried out with two IFs, spaced by 70 MHz, with an effective bandwidth of 42 MHz each. Condon et al. (1998) have calculated the effects of bandwidth depolarisation (their Fig. 23). It is seen that bandwidth depolarisation becomes severe for $|RM| \gtrsim 100$ rad m^{-2}, implying that about 15% of the sources with determined RMs are likely to be significantly affected.

We have checked the possible effect of this depolarisation on our complete sample and, assuming a worst-case scenario, still find that possible changes are within the range of errors of the data extracted from the NVSS. Our conclusions are therefore not altered by this effect.

It is clear from Fig. 2a that the polarisation behaviour of the steep-spectrum sample cannot be fitted with any of the existing simple models of internal or external depolarisation. Internal Faraday dispersion would lead to a depolarisation law

$$m_{\rm obs} = m_0 \cdot \frac{\sin(\phi \cdot \lambda^2)}{\phi \cdot \lambda^2}$$

for a uniform slab (Burn 1966), where $m_{\rm obs}$ is the observed degree of polarisation and m_0 would be that measured in the absence of any Faraday-rotating effects, ϕ is the Faraday depth intrinsic to a source. External depolarisation would be characterized by a law of the form (Tribble 1992)

$$m_{\rm obs} = m_0 \cdot \left(\frac{1 - {\rm e}^{-\frac{y^2}{2} - 4 \cdot \sigma_{RM}^2 \cdot \lambda^4}}{1 + 8 \cdot y^{-2} \cdot \sigma_{RM}^2 \cdot \lambda^4} + {\rm e}^{-\frac{y^2}{2} - 4 \cdot \sigma_{RM}^2 \cdot \lambda^4} \right)^{\frac{1}{2}}.$$

Here, σ_{RM} is the dispersion of a random magnetic field with a Gaussian distribution function of the Rotation Measure *RM*, and

$$y = \frac{L}{HPBW}$$

is the ratio of the scale L of the fluctuations and the angular resolution of the observations, i.e. the telescope *HPBW*. The above equation has the limiting cases of $y \to 0$ and $y \to \infty$, corresponding to the unresolved and resolved foreground screens,

respectively (see Tribble 1992). Whatever the choice of parameters in the above equations, the observed degrees of polarisation of our steep-spectrum sample cannot be reconciled with any of them. In particular, all of the above laws predict a rapid drop of polarisation below a few GHz. A combination of internal and external depolarisation does not help as the fall-off to zero polarisation always wins below a few GHz. Figure 2a shows that the decrease of $m_{\rm obs}$ is roughly linear between $\lambda\lambda$11 and 21 cm, with a stronger increase towards λ2.8 cm.

We have tried to reproduce this behaviour assuming that the bulk of the depolarisation is intrinsic to the source. This can be described with the recipe given by Gardner & Whiteoak (1966), assuming that we measure a superposition of several source components with different Faraday depths and polarised fluxes. This implies that the different components add in the Stokes (*Q*,*U*) plane, with the polarisation properties ($m_{\rm obs}$, χ) resulting in the usual way. Then, if we consider *N* domains with different Faraday depths ϕ_i and flux densities B_i, we obtain (see Eq. (32) in Gardner & Whiteoak 1966)

$$U = \sum \frac{B_i \cdot \sin(\lambda^2 \cdot \phi_i) \cdot \sin(\lambda^2 \cdot \phi_i)}{\lambda^2 \cdot \phi_i} = \sum \frac{B_i \cdot \sin^2(\lambda^2 \cdot \phi_i)}{2 \cdot \lambda^2 \cdot \phi_i}$$

$$Q = \sum \frac{B_i \cdot \sin(\lambda^2 \cdot \phi_i) \cdot \cos(\lambda^2 \cdot \phi_i)}{\lambda^2 \cdot \phi_i} = \sum \frac{B_i \cdot \sin(2 \cdot \lambda^2 \cdot \phi_i)}{2 \cdot \lambda^2 \cdot \phi_i}.$$

Choosing identical amplitudes (flux densities) B_i for *Q* and *U* just implies a polarisation angle of 45° for each of the domains. It now turns out that with the above law, one needs but few different components in order to reproduce the polarisation behaviour as measured by us. The resulting zero-wavelength polarisation angle intrinsic to the source then depends on the relative contribution of emissivities in the (*U*,*Q*) plane.

In Fig. 2b we have superimposed a "model" onto the median values of $m_{\rm obs}$ of the steep-spectrum sources. The model comprises three emissivity components seen by the beam. Their contributions to Stokes *Q* and *U* have been chosen equal for simplicity. Their relative amplitudes B_i and Faraday depths ϕ_i are 28%, 46% and 26%, 200 rad m^{-2}, 30 rad m^{-2} and 3 rad m^{-2}, respectively. It is obvious that the measured $m_{\rm obs}$ can be readily reproduced with just a few components. Adding more components would smooth the curve, but the individual emissivities of further components would be comparatively small. This configuration of polarised domains in a source produces only little Faraday rotation, as can be seen in Fig. 2c. Between zero wavelength and about $\lambda \gtrsim 25$ cm, the polarisation angle rotates by $\sim$23°, then oscillating around this angle. In principle, one would have to account for the redshifts of the individual sources in order to provide a proper interpretation. However, as will be briefly discussed in Sect. 4.4.3, the lack of any correlation with polarisation properties renders such an analysis rather vague, at least at the present time.

If this scenario is real, then most of the observed Faraday rotation must originate in a (uniform) foreground screen, either in the Milky Way or in some intervening extragalactic medium, e.g. thermal and magnetized cluster gas. However, as demonstrated by Clarke et al. (2001), the corresponding "impact parameter" of the line-of-sight through an average galaxy cluster needs to be small ($\leq$500 kpc) in order to produce significant Faraday rotation. It is therefore likely that the observed Faraday rotation is Galactic. This sounds also reasonable in view of large corrections that would have to be made otherwise, i.e. if we would scale the observed *RM*s by $(1+z)^2$ to go into the rest frame. This would partly result in unrealistically large intrinsic *RM*s. In fact, as mentioned in Sect. 4.3, the trend for higher *RM*s at lower Galactic latitudes seen in our data corroborates this conjecture.

We now briefly discuss whether the above considerations are meaningful and realistic. The three components with which the median values can obviously be readily explained using a superposition of uniform slabs could reflect different source components, such as the jets, hotspots and lobes, or different regions within the lobes. If a radio source is located in a hot coronal gas, these source components will be immersed in local environments with different Faraday depths. It is clear that the short-wavelength behaviour of the degrees of polarisation is controlled by the component with the highest Faraday depth (200 rad m^{-2}), while at long wavelengths it is the low Faraday depth (3 rad m^{-2}) which governs. The value of the latter cannot be strongly changed without causing too strong a deviation from the observed $m_{\rm obs}$, in particular at λ21 cm.

4.3.2. Sources with good signal-to-noise

In this subsection we discuss the polarisation behaviour of those sources that have adequate signal-to-noise ratios of the polarised flux densities. We have identified a total of 26 such sources for which the measured degrees of polarisation are $\gtrsim$10 times as large as the measured errors on average. The behaviour is not much different from that of the "complete sample", requiring again three components with similar parameters.

4.3.3. Trends with redshift?

One of the most intriguing questions is naturally whether there is any relation between the polarisation properties and redshift. Redshifts are available for a fair subsample (132 sources). A visual inspection of the plots of $m_{\rm obs}(\lambda)$ was made to disclose any correlation with redshift. No clear relation was found. As already noted by Mesa et al. (2002), there might be two effects at work producing some kind of "degeneracy": given that one would not expect any dependence of the *intrinsic* (i.e. rest-frame) degree of polarisation on radio luminosity, one might expect an apparent positive correlation between the *observed* degrees of polarisation and luminosity, since the most luminous sources are expected to have the higher redshifts. On the other hand, cosmic expansion gives rise to an apparent reduction of the *RM*s as measured by the observer. This scenario renders a variety of polarisation properties going one or the other way.

5. Conclusions

In this paper we have presented the results of the measurement of linear polarisation of a subsample of radio sources culled from the B3-VLA survey, carried out with the Effelsberg

100-m telescope at λλ11.1, 6.3 and 2.8 cm, and extracted from the NVSS at λ21 cm. We could not find any correlation with either redshift or radio luminosity, in line with the findings of Mesa et al. (2002). We find that flat-spectrum sources are significantly less polarised than the steep ones at 10.5 GHz. A trend is seen for sources with larger linear sizes to be more strongly polarised. CSSs exhibit much stronger depolarisation than non-CSSs. Flat-spectrum sources are characterized by almost constant, and low, degrees of polarisation over the whole wavelength range studied here.

The most conspicuous result of our study is that the measured degrees of polarisation for the steep-spectrum sources as a function of wavelength are in disagreement with existing models of external depolarisation or intrinsic Faraday dispersion. The decrease of the degree of polarisation is almost linear with wavelength and does not drop to zero at lower frequencies, as expected.

We consider an intrinsic process producing the observed depolarisation, involving essentially three source components with different emissivities and Faraday depths. If these considerations are correct, then the Faraday rotation must arise from a foreground screen, which is likely to be the magneto-ionic medium in our own Milky Way. This can possibly be checked by multi-frequency observations at high-angular resolutions. If the Faraday screen is mainly intrinsic to the source, the *RM*s should vary across the target, while a Galactic foreground rotation would have the same effect in different regions of the source.

Our polarisation data have aided the investigation of any possible influence of the population of polarised radio sources to the polarised component of the cosmic microwave background (Mesa et al. 2002).

Acknowledgements. Part of this work was supported by the Deutsche Forschungsgemeinschaft, grant KL533/4-2, and by the European Commission, TMR Programme, Research Network Contract ERBFMRXCT97-0034 'CERES'. KHM was supported by a Marie-Curie-Fellowship of the European Commission. UK is grateful to the CNR for the warm hospitality during several stays throughout this work. Most of the data presented in this paper are based on observations with the 100-m telescope of the MPIfR (Max-Planck-Institut für Radioastronomie) at Effelsberg.

We thank the referee for useful criticism, which improved the discussion of the results.

References

Baars, J. W. M., Genzel, R., Pauliny-Toth, I.I.K., & Witzel, A. 1977, A&A, 61, 99
Burn, B. J. 1966, MNRAS, 133, 67
Clarke, T. E., Kronberg, P. P., & Böhringer, H. 2001, ApJ, 547, L111
Condon, J. J., Cotton, W. D., Greisen, E. W., et al. 1998, AJ, 115, 1693
Fanti, C., Fanti, R., Dallacasa, D., et al. 1995, A&A, 302, 317
Fanti, C., Pozzi, F., Dallacasa, D., et al. 2001, A&A, 369, 380
Ficarra, A., Grueff, G., & Tomassetti, G. 1985, A&AS, 59, 255
Gardner, F. F., & Whiteoak, J. B. 1966, ARA&A, 4, 245
Gregorini, L., Vigotti, M., Mack, K.-H., Zönnchen, J., & Klein, U. 1998, A&AS, 133, 129 (Paper I)
Kronberg, P. P., & Simard-Normandin, M. 1976, Nature, 263, 653
Mack, K.-H., Klein, U., O'Dea, C. P., & Willis, A. G. 1997, A&AS, 123, 423
Mesa, D., Baccigalupi, C., De Zotti, G., et al. 2002, A&A, 396, 463
Saikia, D. J. & Salter, C. J. 1988, ARA&A, 26, 93
Simard-Normandin, M., Kronberg, P. P., & Neidhöfer, J. 1981, A&AS, 43, 19
Sofue, Y., Fujimoto, M., & Kawabata, K.-A. 1979, PASJ, 31, 125
Strom, R. G. 1973, A&A, 25, 203
Tribble, P. C. 1992, MNRAS, 256, 281
van Breugel, W., Miley, G., & Heckman, T. 1984, AJ, 89, 5
Vigotti, M., Djorgovski, S. G., Thompson, D., et al. 1996, in Extragalactic Radio Sources, ed. R. Ekers, C. Fanti, & L. Padrielli (Dordrecht: Kluwer), Proc. IAU Symp., 175, 519
Vigotti, M., Grueff, G., Perley, R., Clark, B. G., & Bridle, A.J. 1989, AJ, 98, 419
Vigotti, M., Gregorini, L., Klein, U., & Mack, K.-H. 1999, A&AS, 139, 359 (Paper II)
Wardle, J. F. C., & Kronberg, P. P. 1974, ApJ, 194, 249
Wielebinski, R., & Krause, F. 1993, A&ARv, 4, 449